Exploratory Study into the Use of Nanotechnology for Reinforcement of Weak Soils

Xianming Shi, Ph.D., P.E.

Associate Professor, Washington State University

August 10, CESTiCC Annual Workshop

Outline

- Acknowledgements
- Background
- Influence of Releasing Graphene Oxide into A Clayey Sand
- Mechanism for soil reinforcement by electro-osmosis in presence of calcium chloride
- Effect of Nanomaterials and Electrode Configuration on Soil Consolidation by Electroosmosis
- Future direction of this work
- Q & A

电化学方法加固软土的主要动电学现象

Na^+, K^+ ,Ca^{2+}, Mg^{2+}, Fe^{3+}

Cl^-, SO_4^{2-}, PO_3^{2-}, NO_3^-, CO_3^{2-}

电渗：由电泳或电迁移导致的水的流动。滑动面的土壤强度可能因电渗诱导的湿度变异而改变。

电迁移：阴离子/阳离子在电场下的迁移

电泳：

表面带电固体颗粒的迁移

电解及其它电化学反应：可能导致电极附近酸化或碱化及其它环境风险，

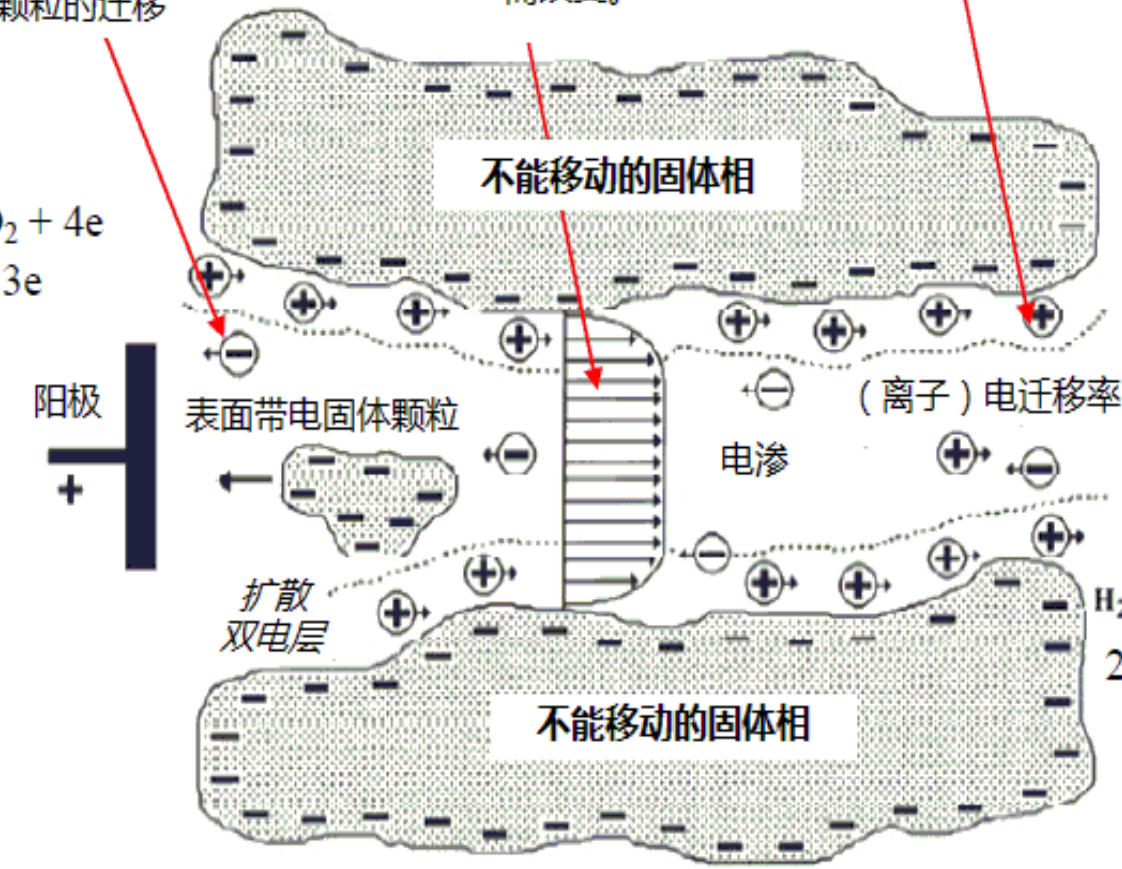

$2H_2O \rightarrow 4H^+ + O_2 + 4e$

$Al \rightarrow Al^{3+} + 3e$

$H_2O \Leftrightarrow H^+ + OH^-$

$2H_2O + O_2 + 4e \rightarrow 4OH^-$

$2H^+ + 2e \rightarrow H_2$

RSC Advances

PAPER

Cite this: *RSC Adv.*, 2017, 7, 18060

Influence of releasing graphene oxide into a clayey sand: physical and mechanical properties

Guo-Xiang Zhou,[abc] Jing Zhong,*[ab] Heng Zhang,[c] Xinhua Hu,[c] Jianlin Wu,[c] Nikhil Koratkar[d] and Xianming Shi *[ce]

Table 1 Physical properties of the soil (clayey sand, SC)

Property	Value
Specific gravity	2.04
Liquid limit	26.2%
Plastic limit	16.1%
Plasticity index	10.1
Average particle size	~0.2 mm
Granularity	≤3 mm

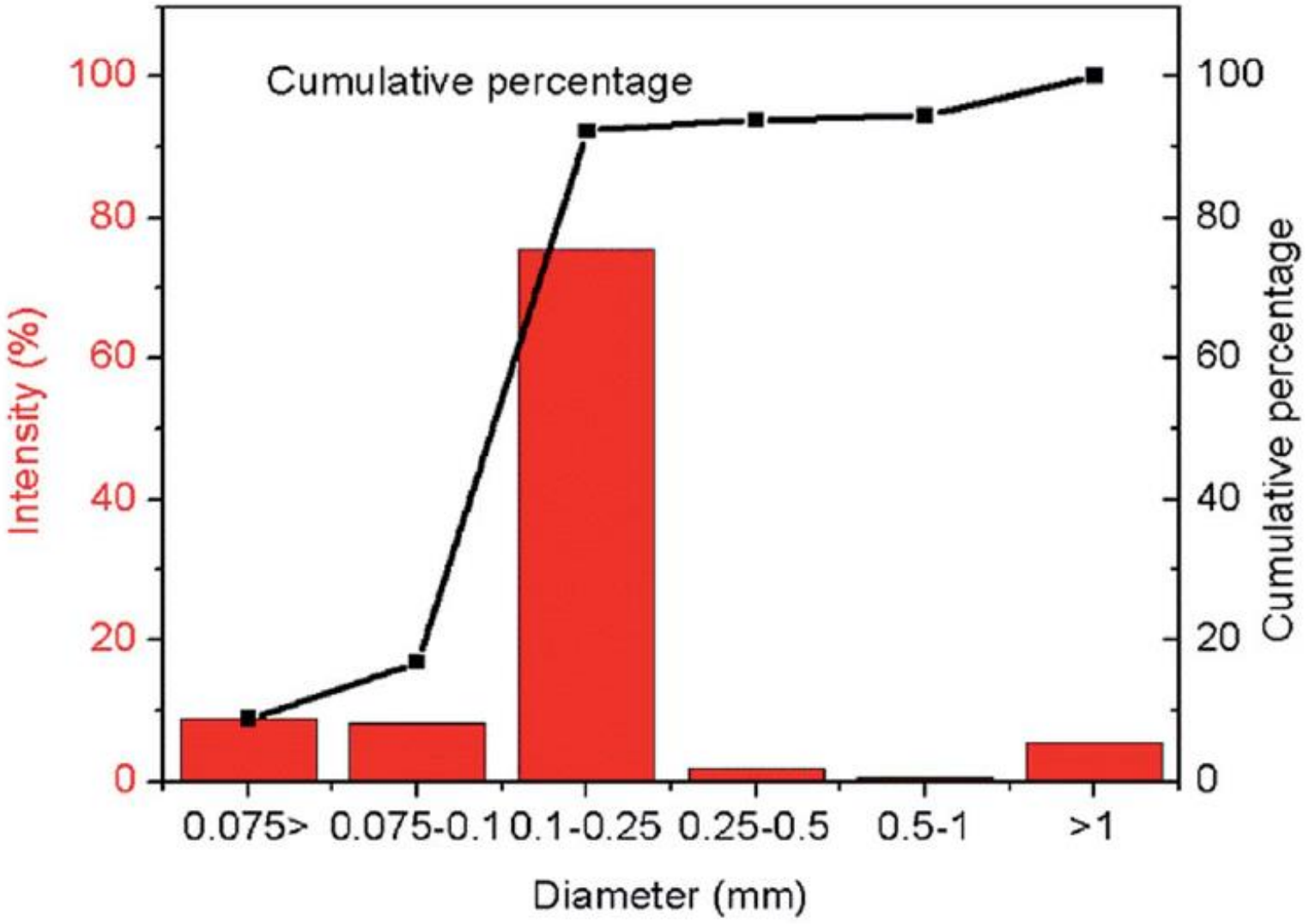

Fig. 1 Gradation curve of the soil used in this study.

Table 2 Chemical composition of the soil, measured by XRF

Compound	Concentration (%)
SiO_2	49.083
Al_2O_3	17.669
Fe_2O_3	4.098
K_2O	2.524
CaO	1.228
MgO	0.718
TiO_2	0.521
P_2O_5	0.105
MnO	0.089
Na_2O	0.061
BaO	0.049
SO_3	0.044
ZrO_2	0.025
CeO_2	0.020
ZnO	0.011
Rb_2O	0.009
Cr_2O_3	0.007
SrO	0.005
CuO	0.004
NiO	0.003
Ga_2O_3	0.002

The water content in the soil was controlled at ~25 wt%.

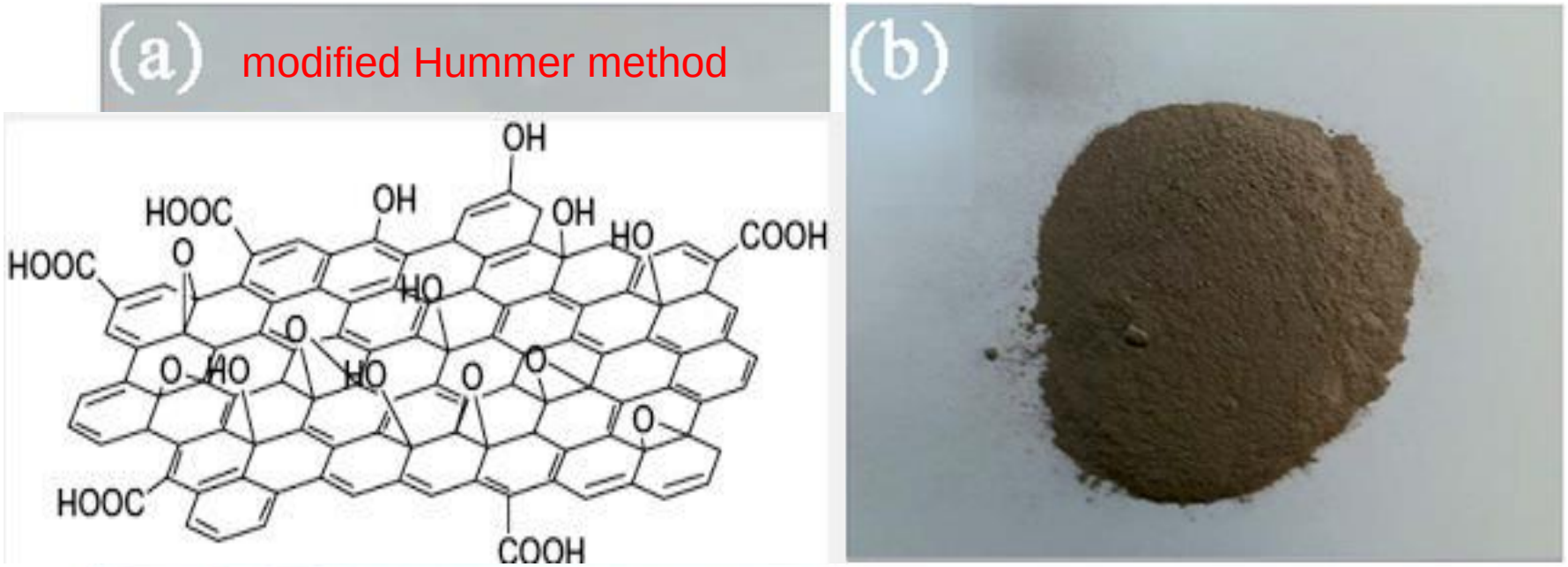

Fig. 2 (a) GO solution with different concentrations; (b) a sample of the soil.

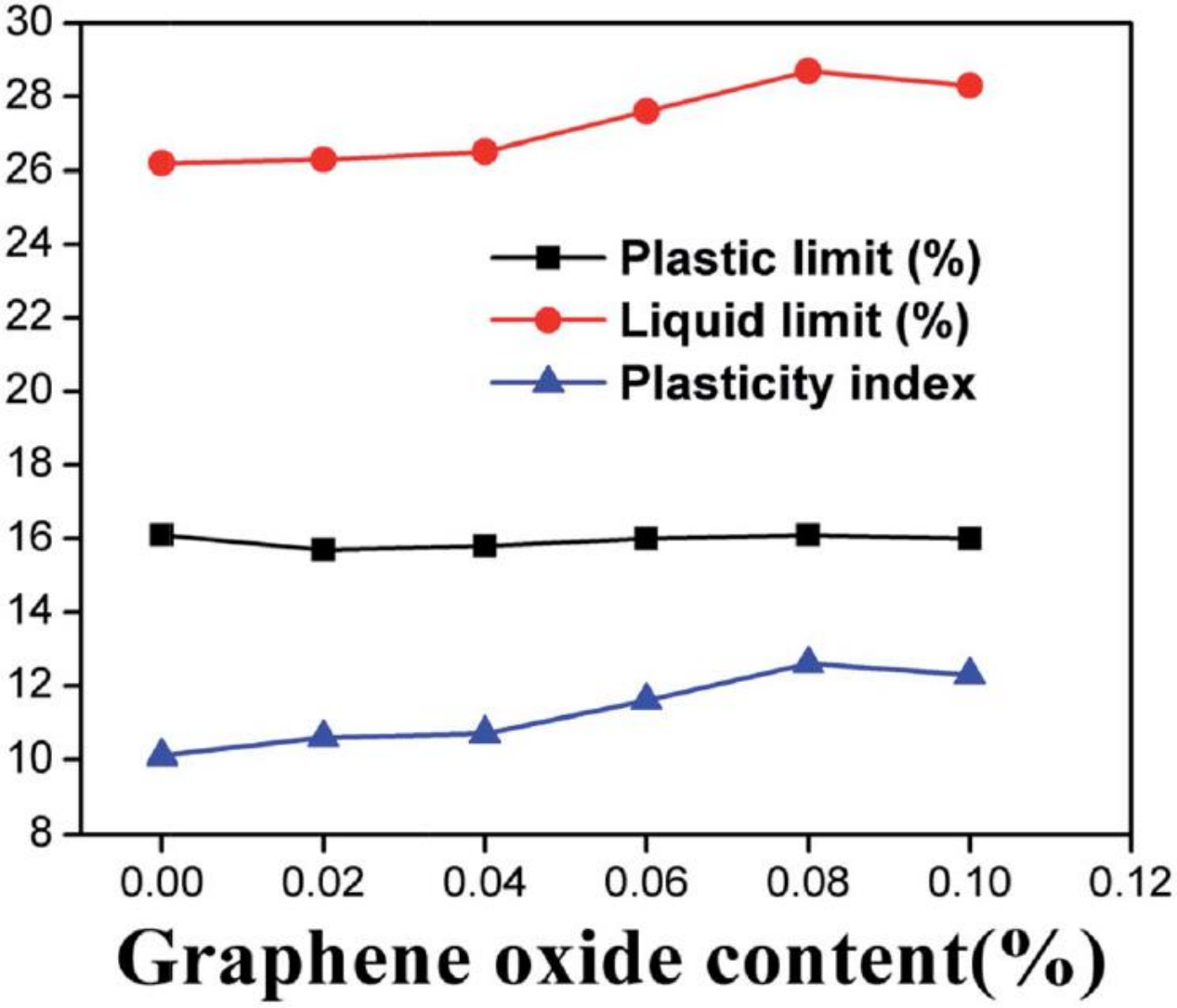

Fig. 3 Property indices of the clayey sand as a function of GO content.

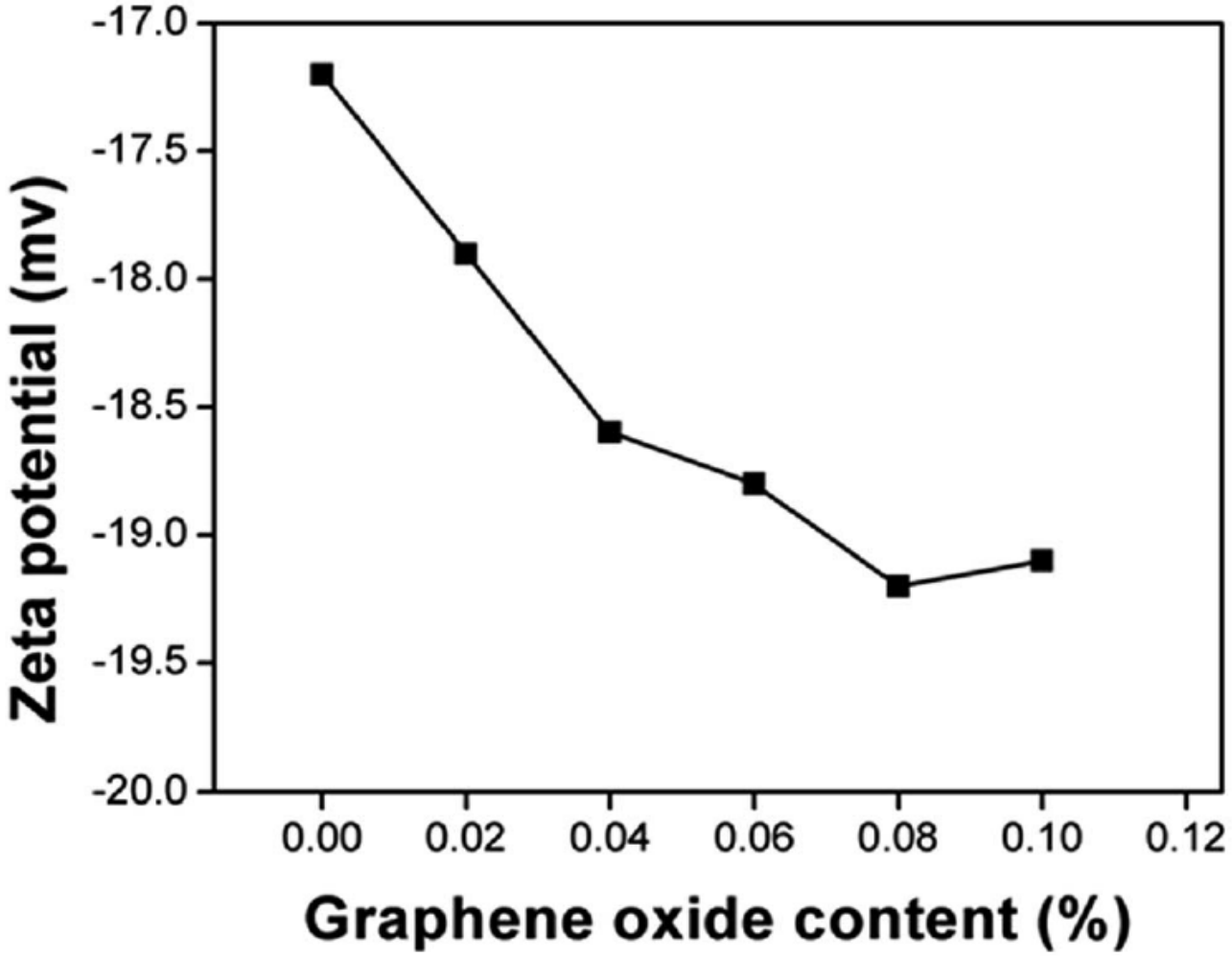

Fig. 4 Zeta potential of the soil as a function of GO content (by weight). The zeta potential of GO in aqueous solution with pH value of 7 is ~30.

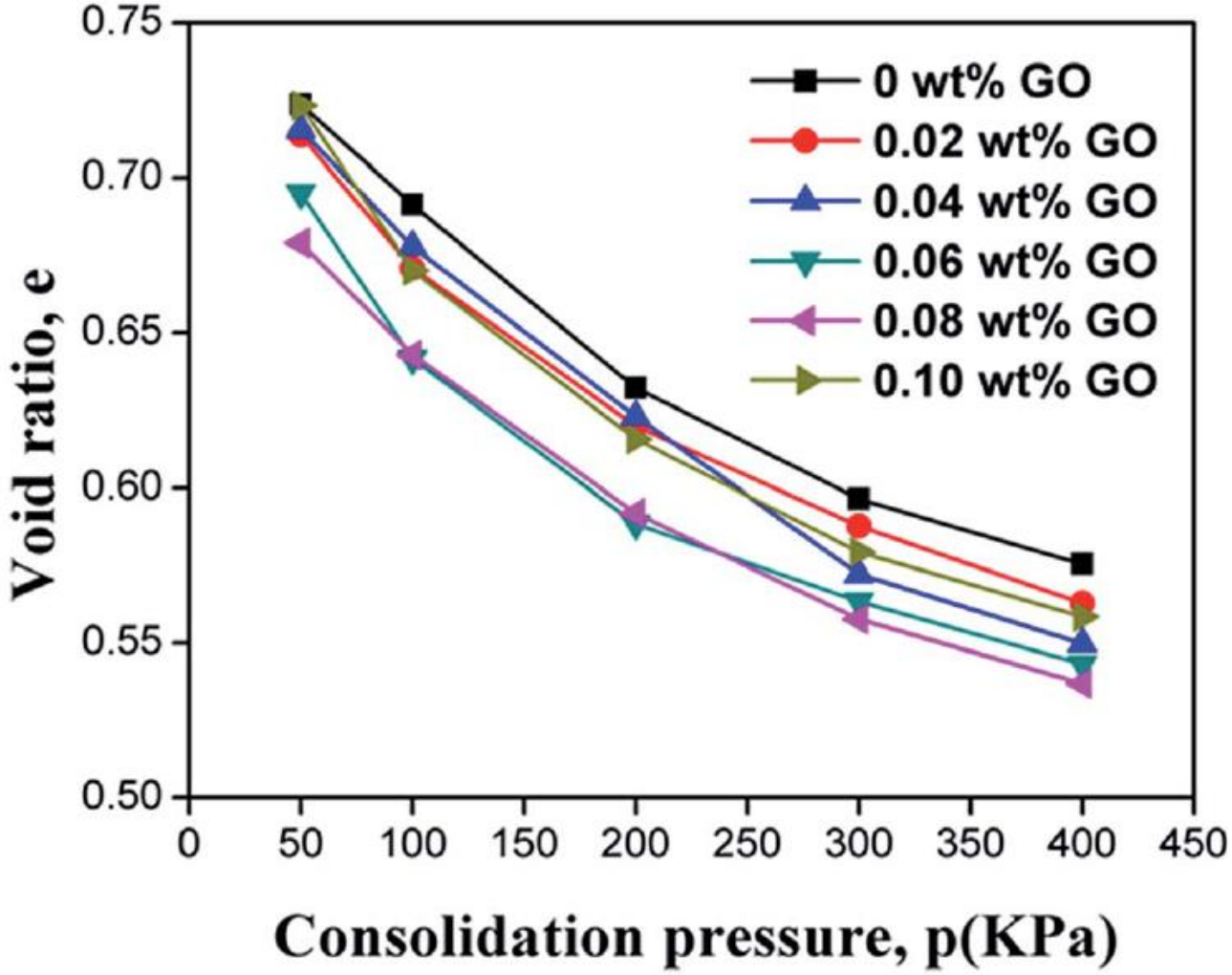

Fig. 5 Compression curves (e–p relationships) of the soil samples.

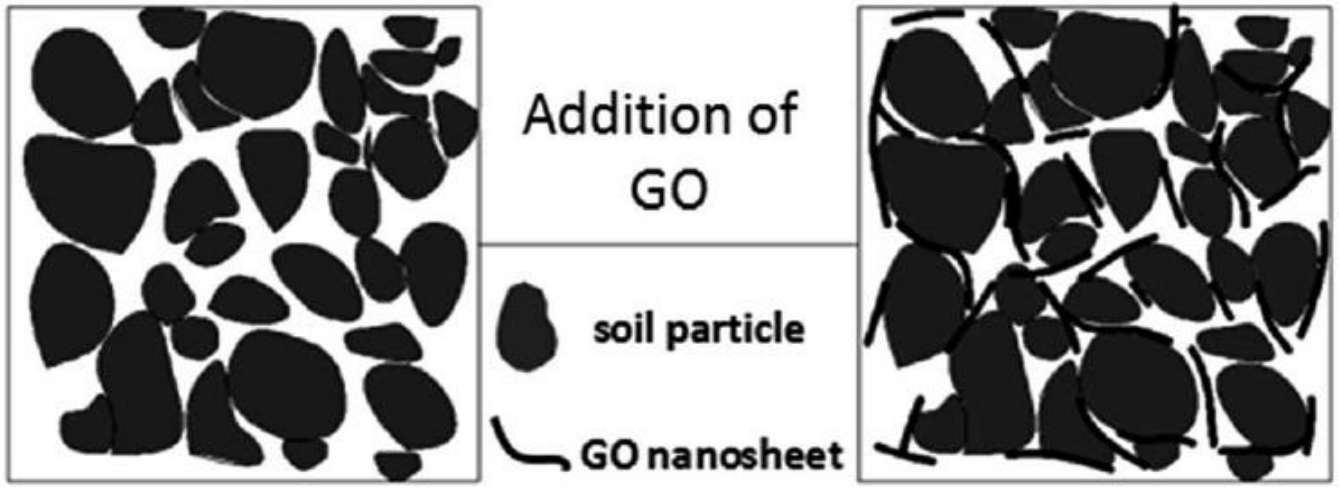

Fig. 6 Schematic illustration of GO nanosheets integrated with soil particles.

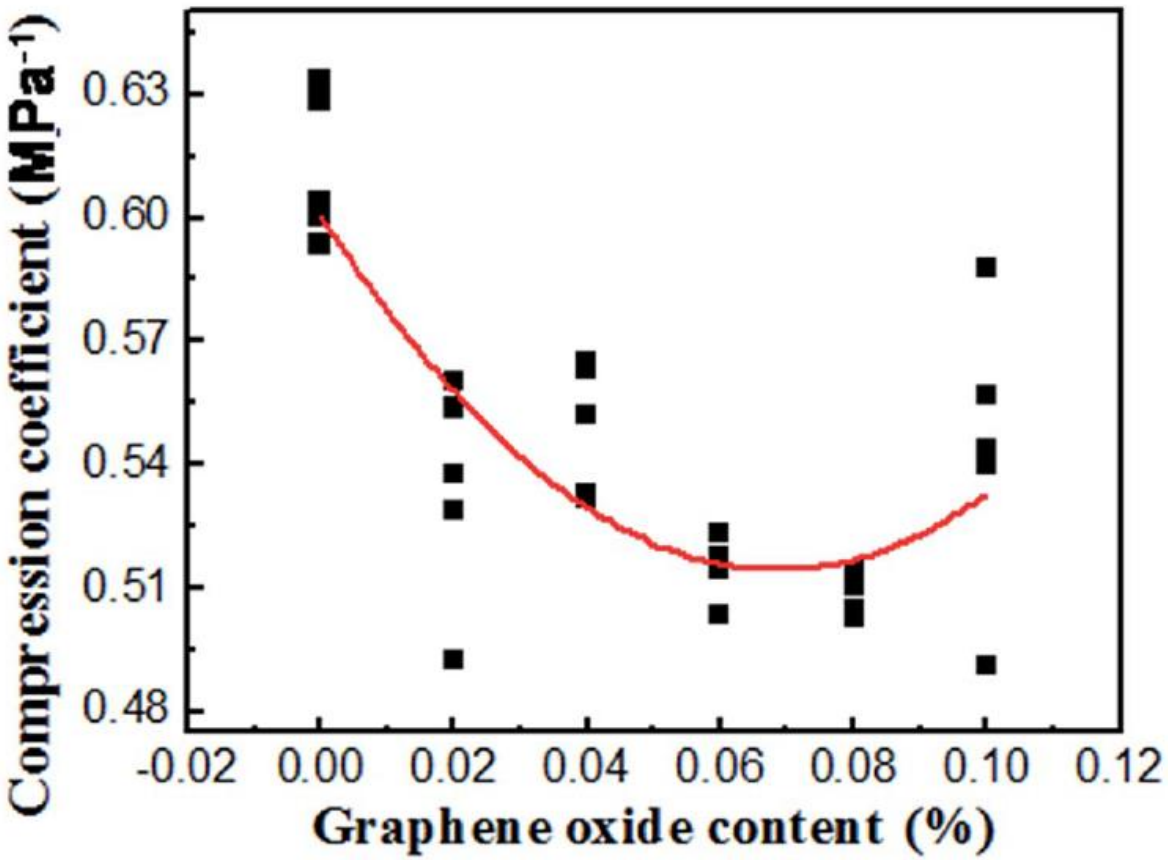

Fig. 7 The relationship between the compression coefficient (α_{1-2}) and GO content.

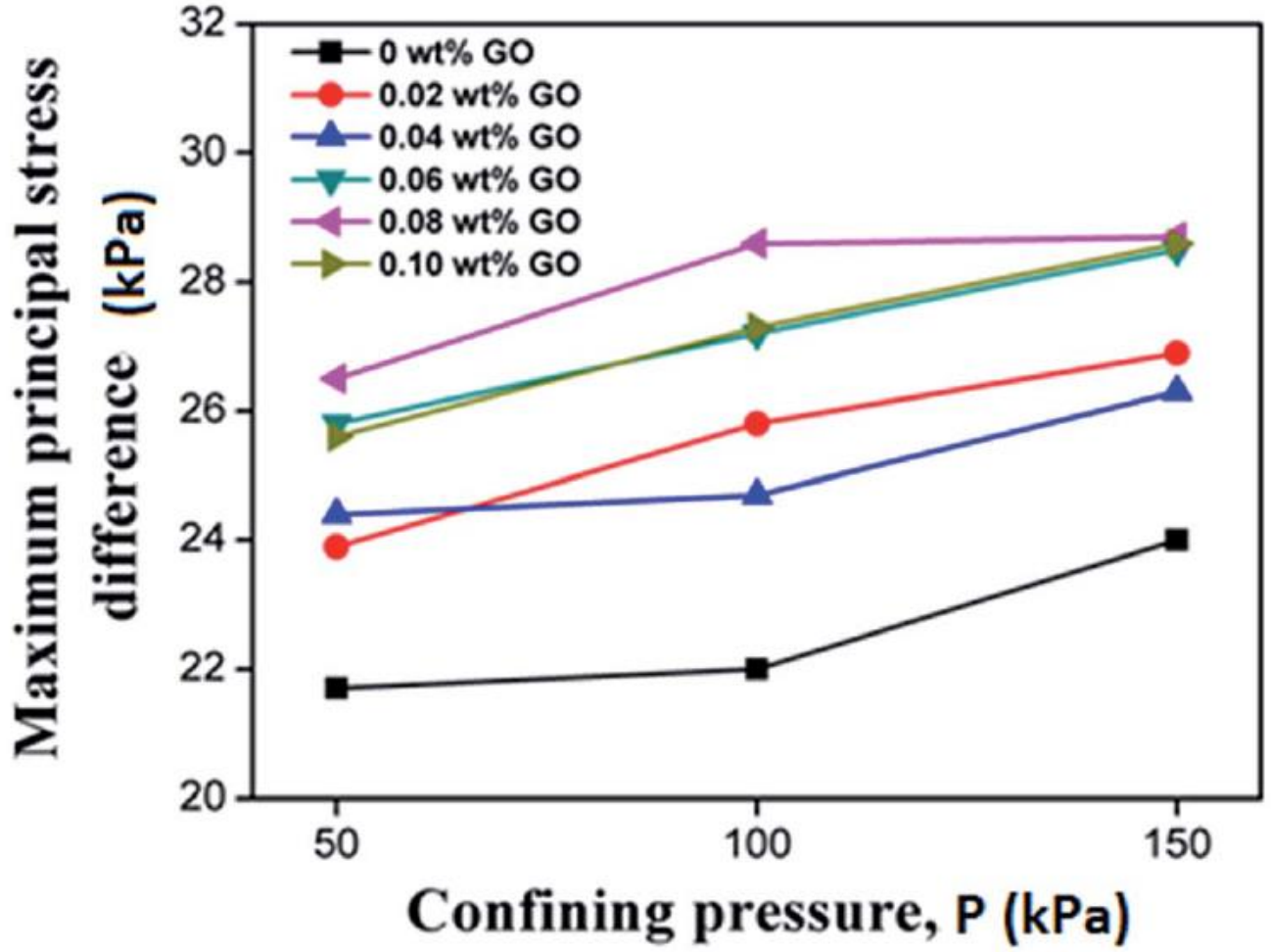

Fig. 8 The relationship between the confining pressure and the maximum principal stress difference.

Table 3 The cohesion C and angle of internal friction φ of specimens

Content (%)	0	0.02	0.04	0.06	0.08	0.1
Cohesion, C (kPa)	10.02	11.13	11.5	12.69	12.72	11.91
φ (°)	0.65	0.84	0.54	0.4	0.63	0.85

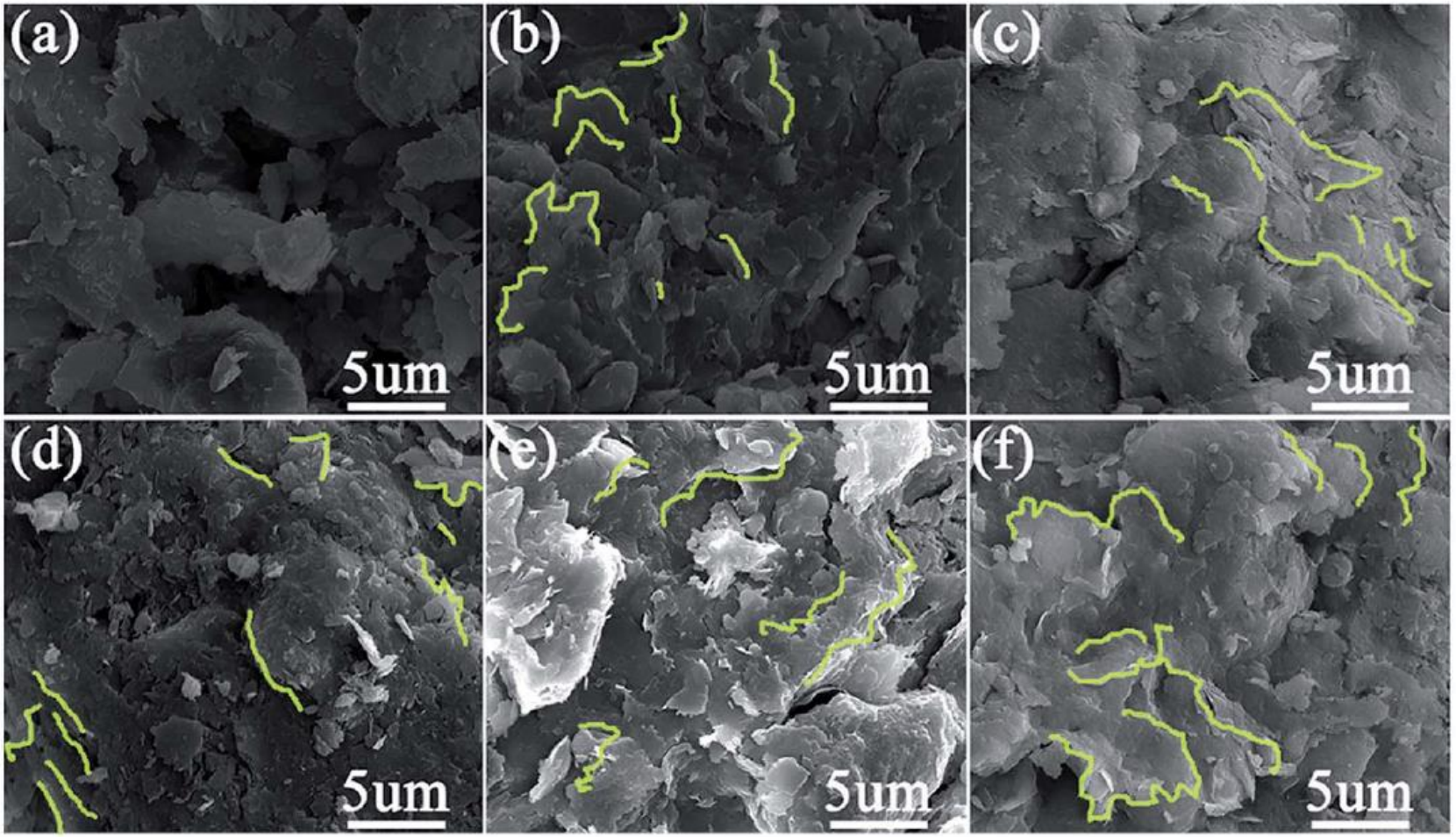

Fig. 9 SEM images of soil samples reinforced by various content of GO:

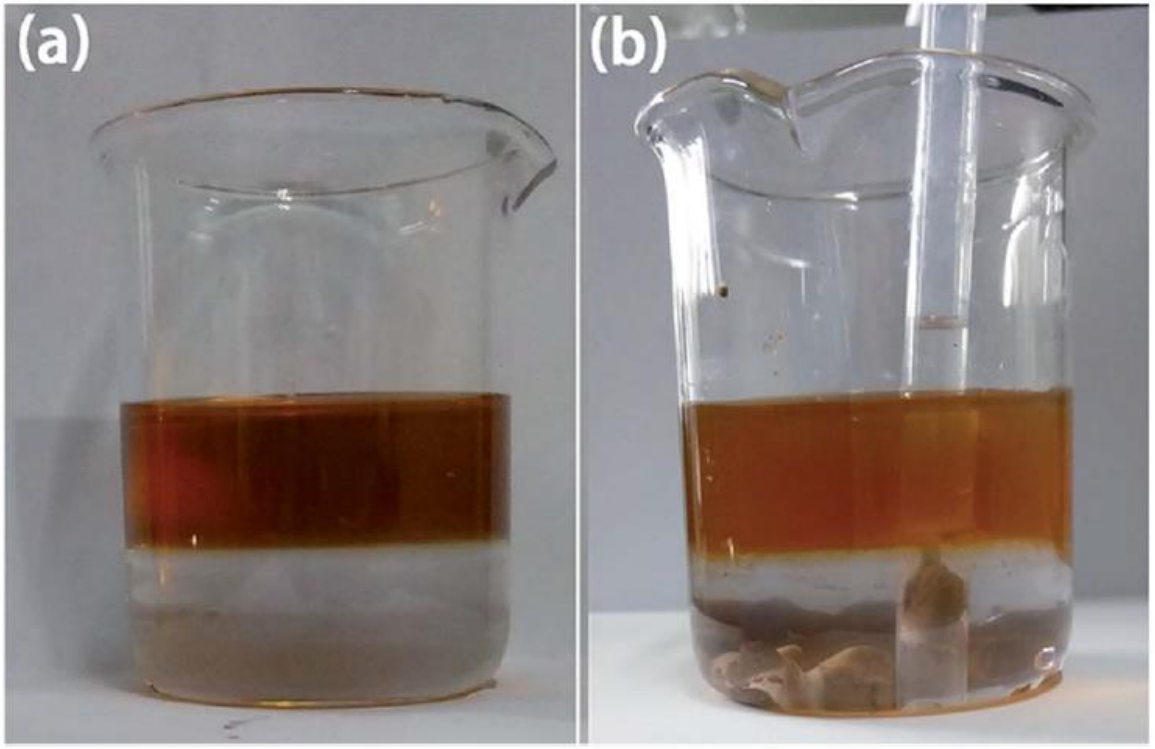

Fig. 10 Images for the two layers of immiscible liquid (GO solution/ dichloromethane), before (a) and after (b) the sedimentation test of soil particles.

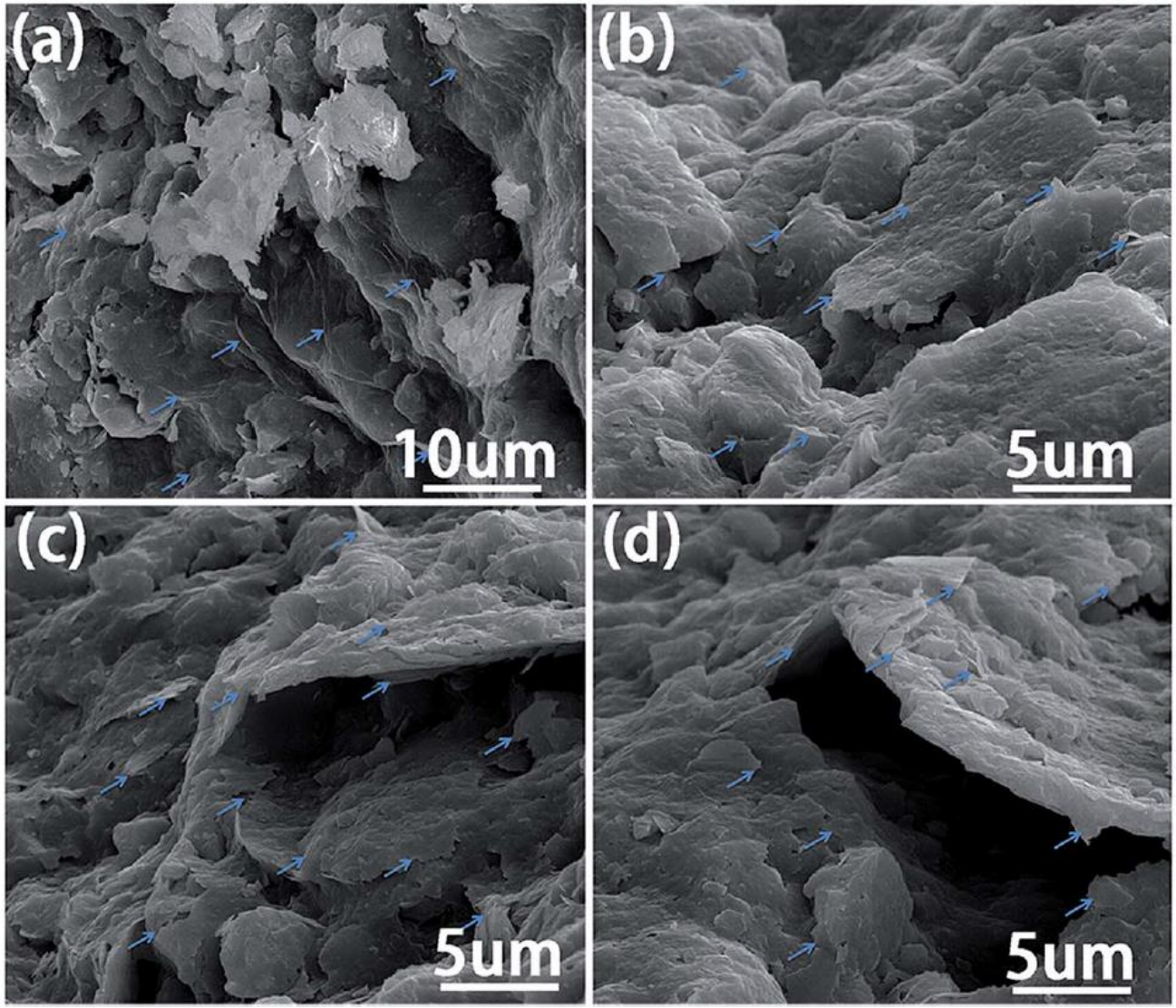

Fig. 11 SEM images of the soil particles after the sedimentation test illustrated in Fig. 10.

Conclusions

- We have for the 1st time the effects of GO on the physical and mechanical properties of a soil.
- With only a small amount of GO (no more than 0.08 wt.%), the properties of the clayed sand can be modified significantly, in terms of liquid limit, plasticity index, compressibility, and undrained shear strength.
- The effectiveness of GO as a soil modifier stems from its extremely high specific surface area (2600 m^2/g) and very stable dispersion in water. The hydrophilic GO sheets intercalate into the spaces between the soil particles and help to increase the bound water content, leading to less compressibility of the clayey sand.

Mechanism for soil reinforcement by electro-osmosis in presence of calcium chloride

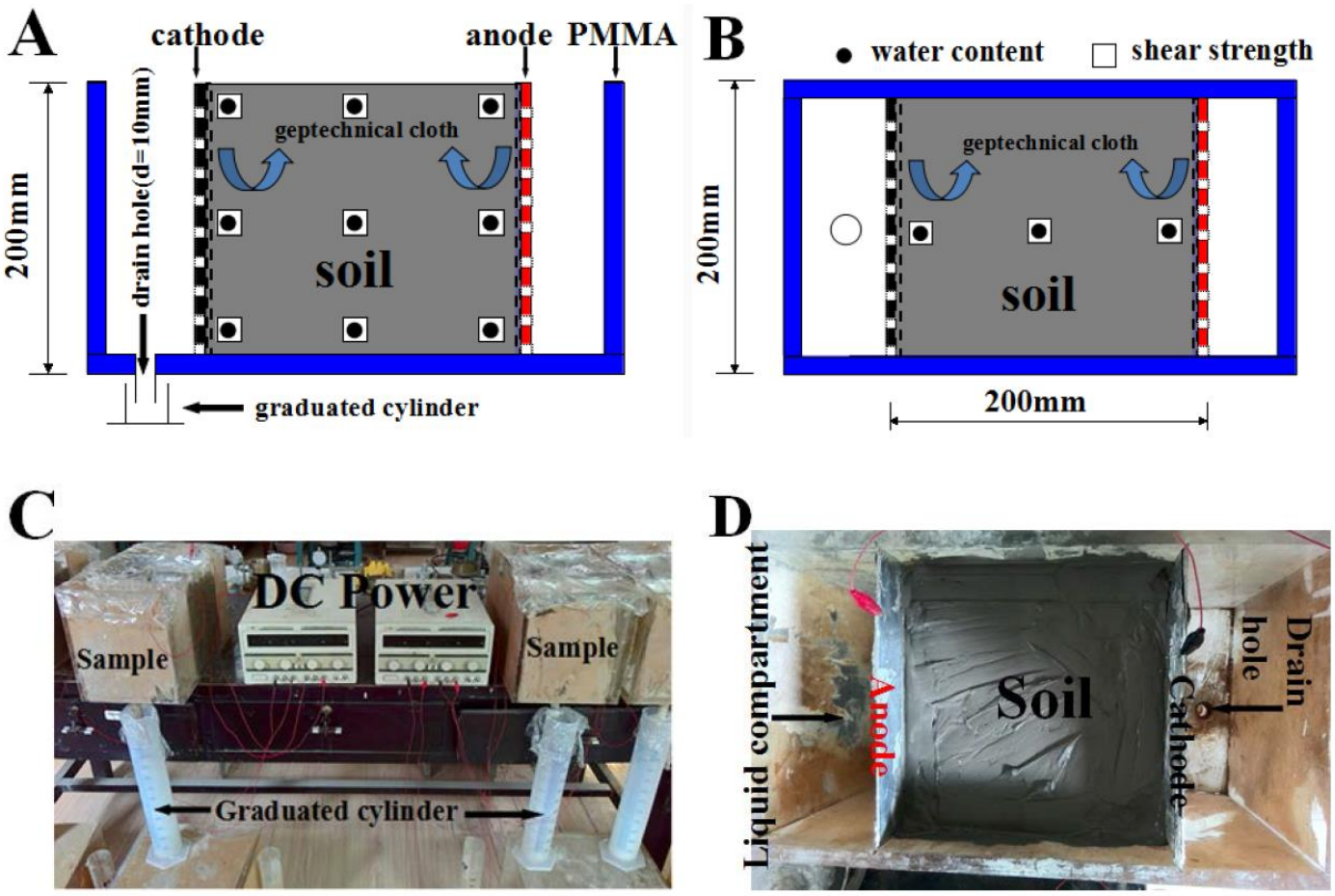

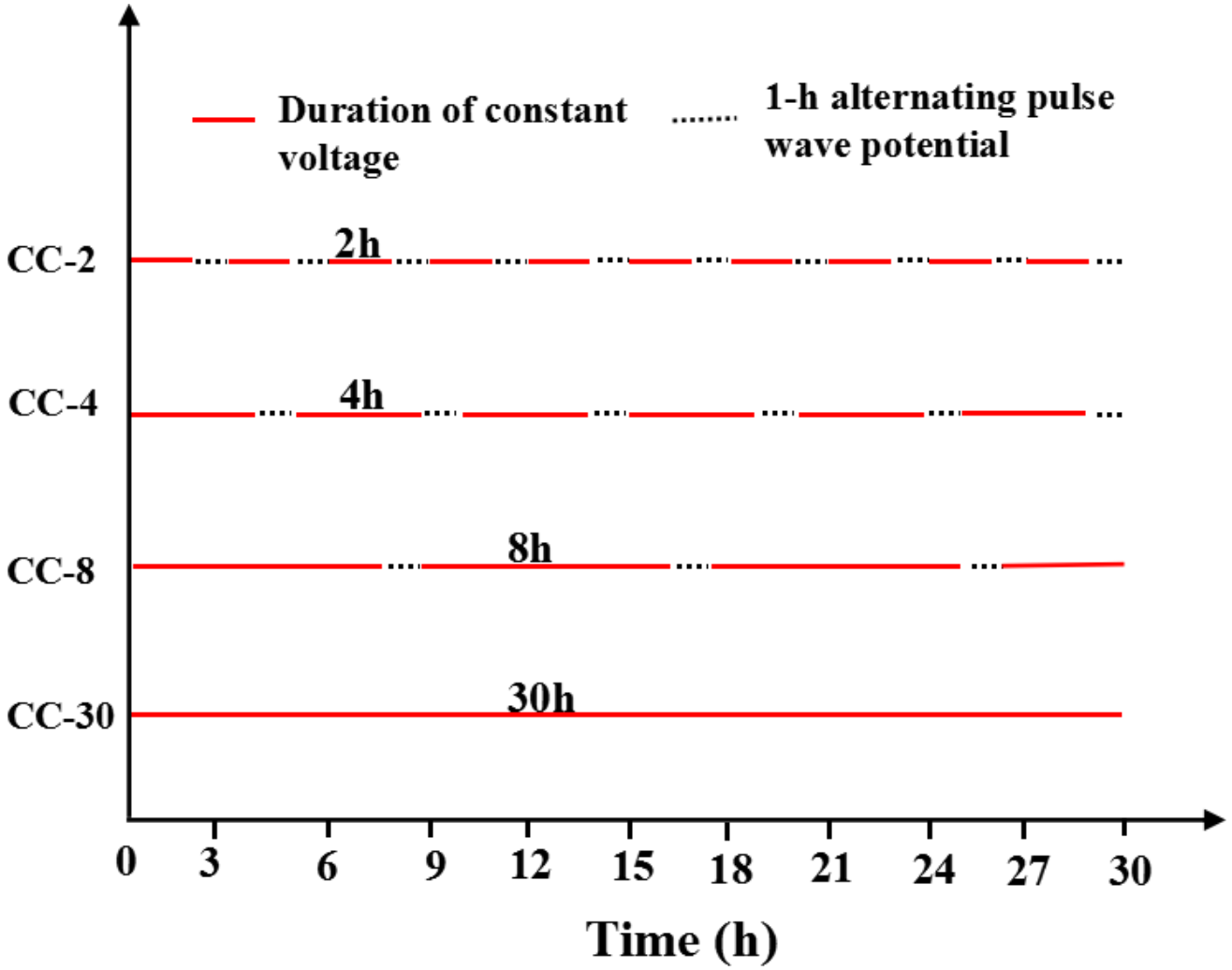

Figure 2. Alternating pulse wave potentials.

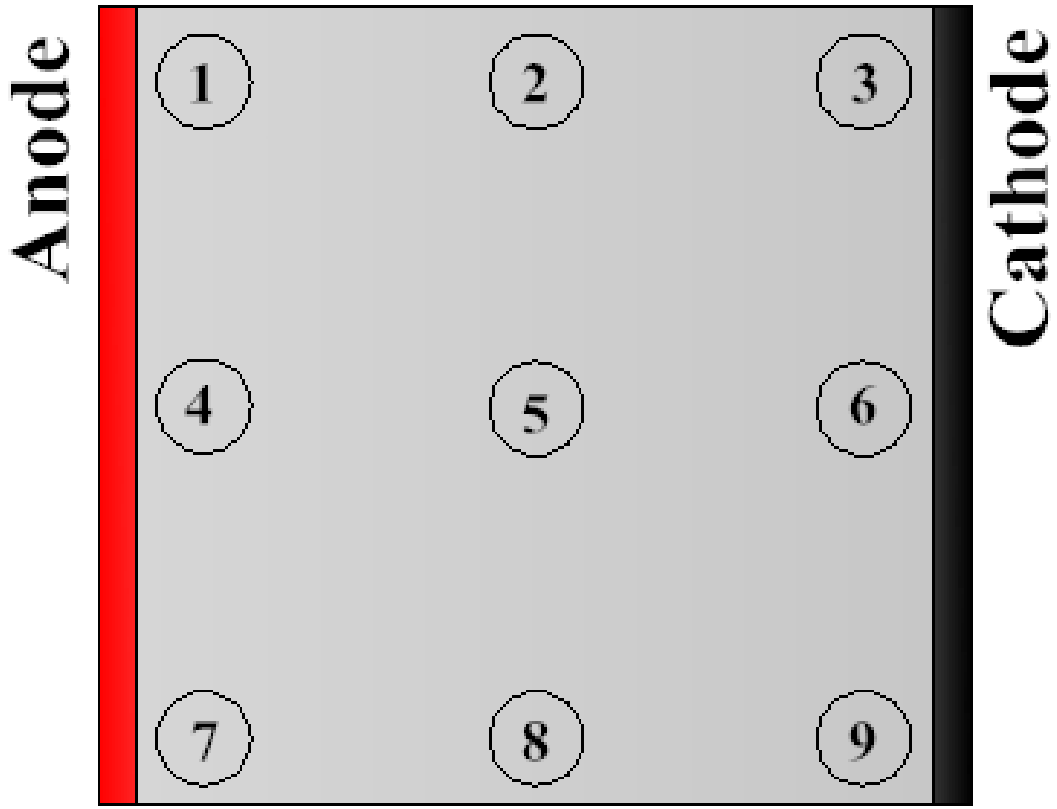

Figure 3. Positions for samples tested for water content and mechanical property.

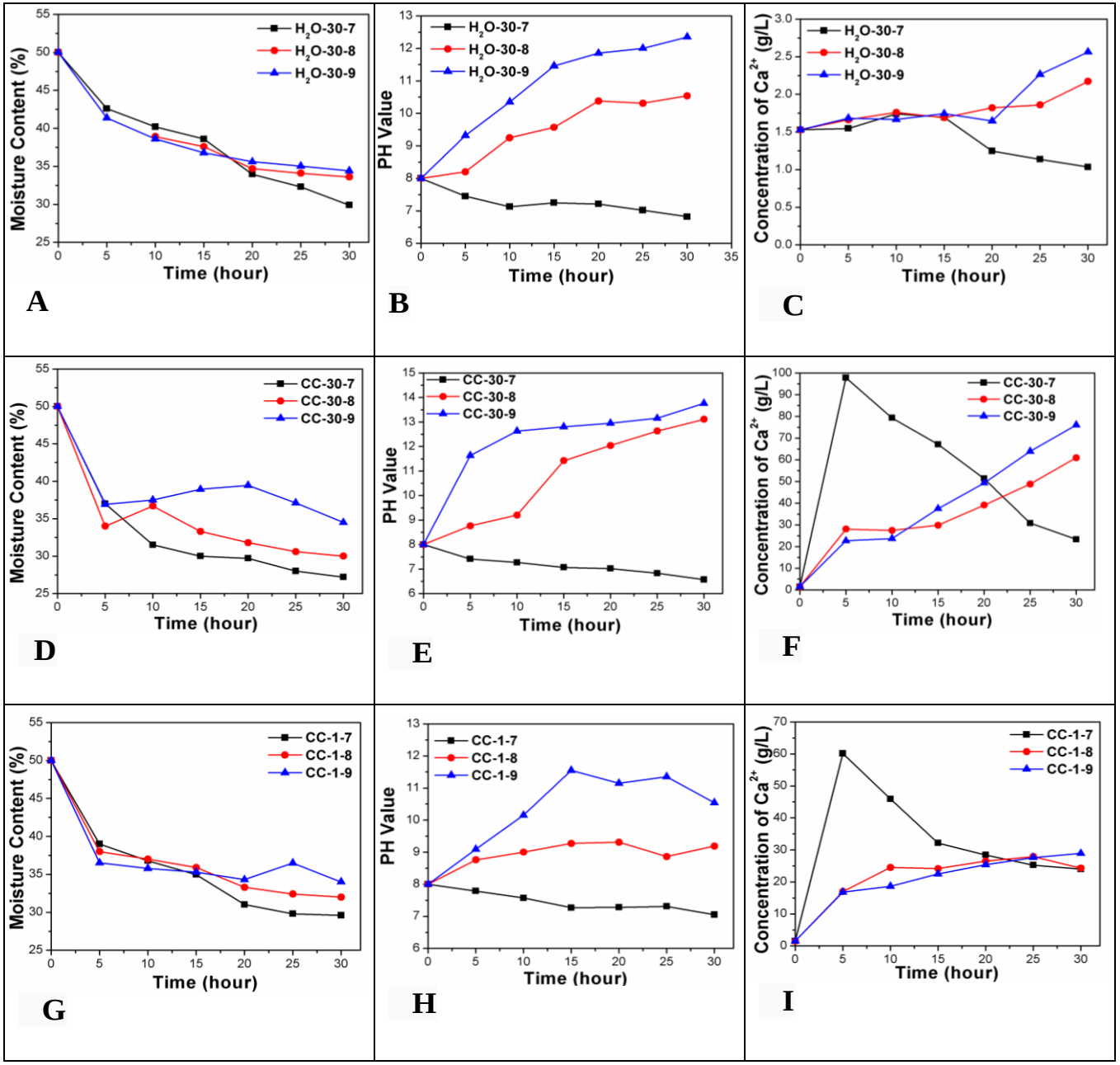

Figure 4. Variation of moisture content, pH value and free Ca^{2+} concentration with treatment time and soil location. (A-C): H_2O-30; (D-F): CC-30; (G-I): CC-1.

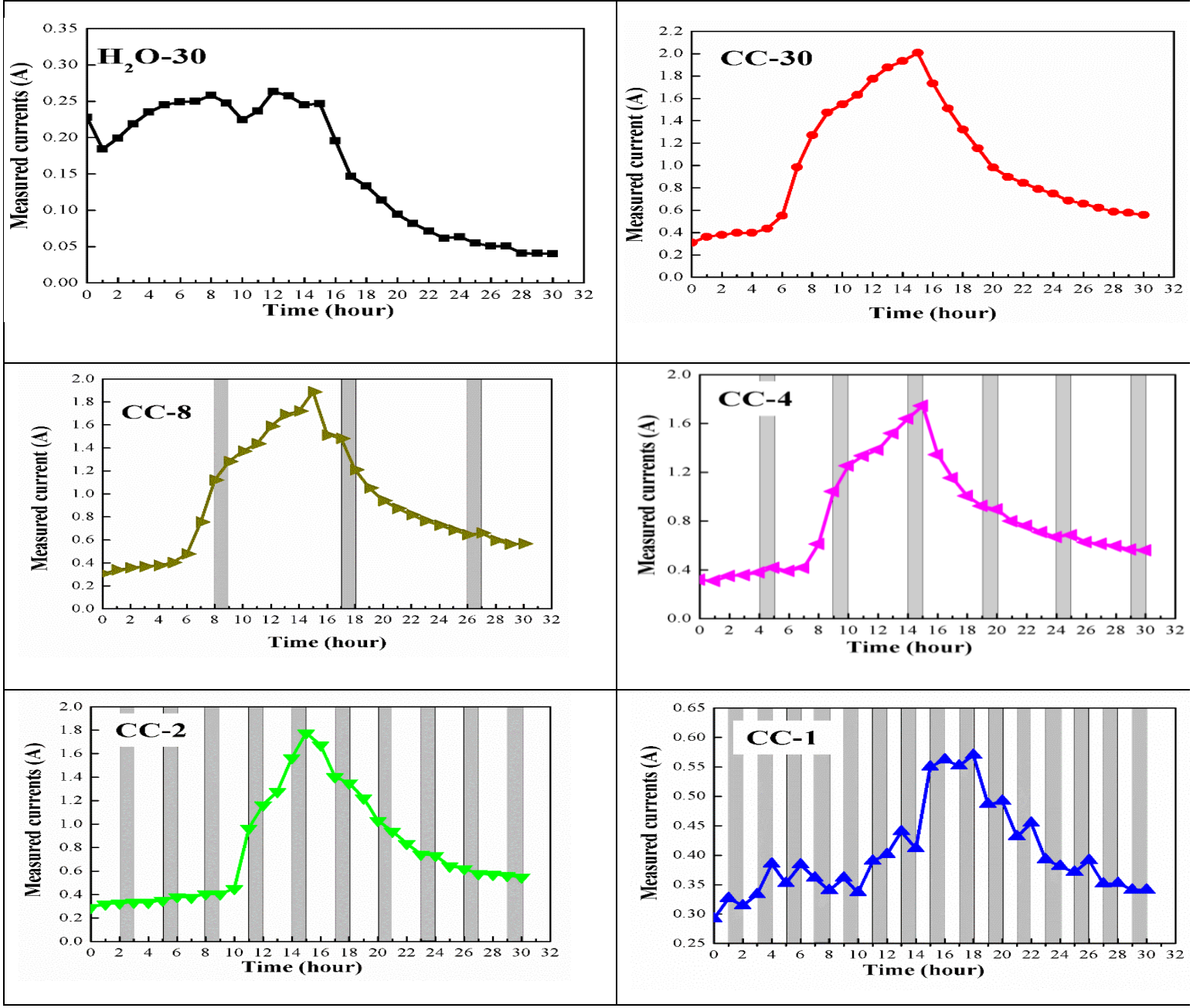

Figure 5. Temporal evolution of electric current with time during electro-osmosis, with electrolyte or water removed at 15 h.

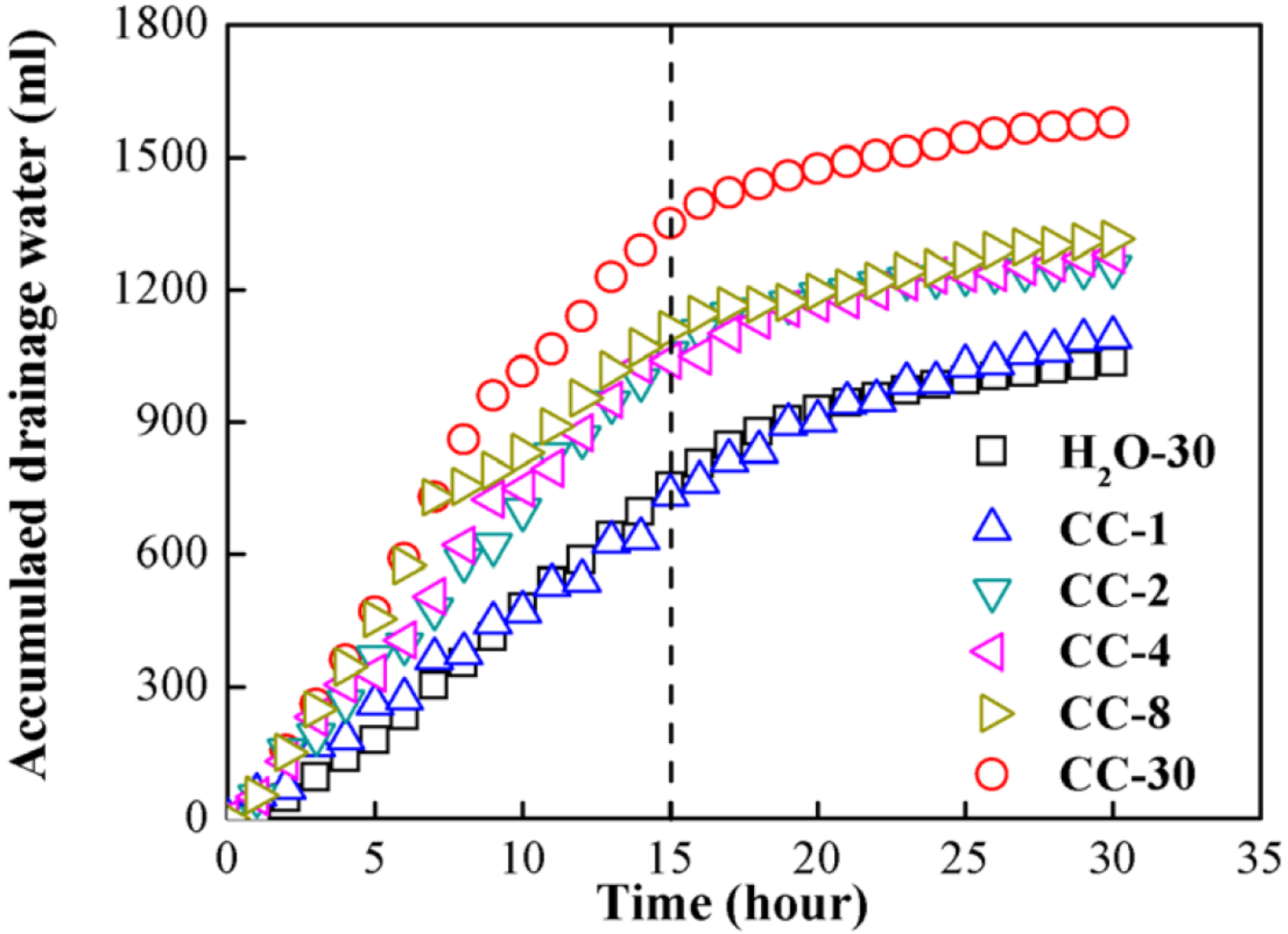

Figure 6. Temporal evolution of cumulative amount of drained water, with electrolyte or water removed at 15 h.

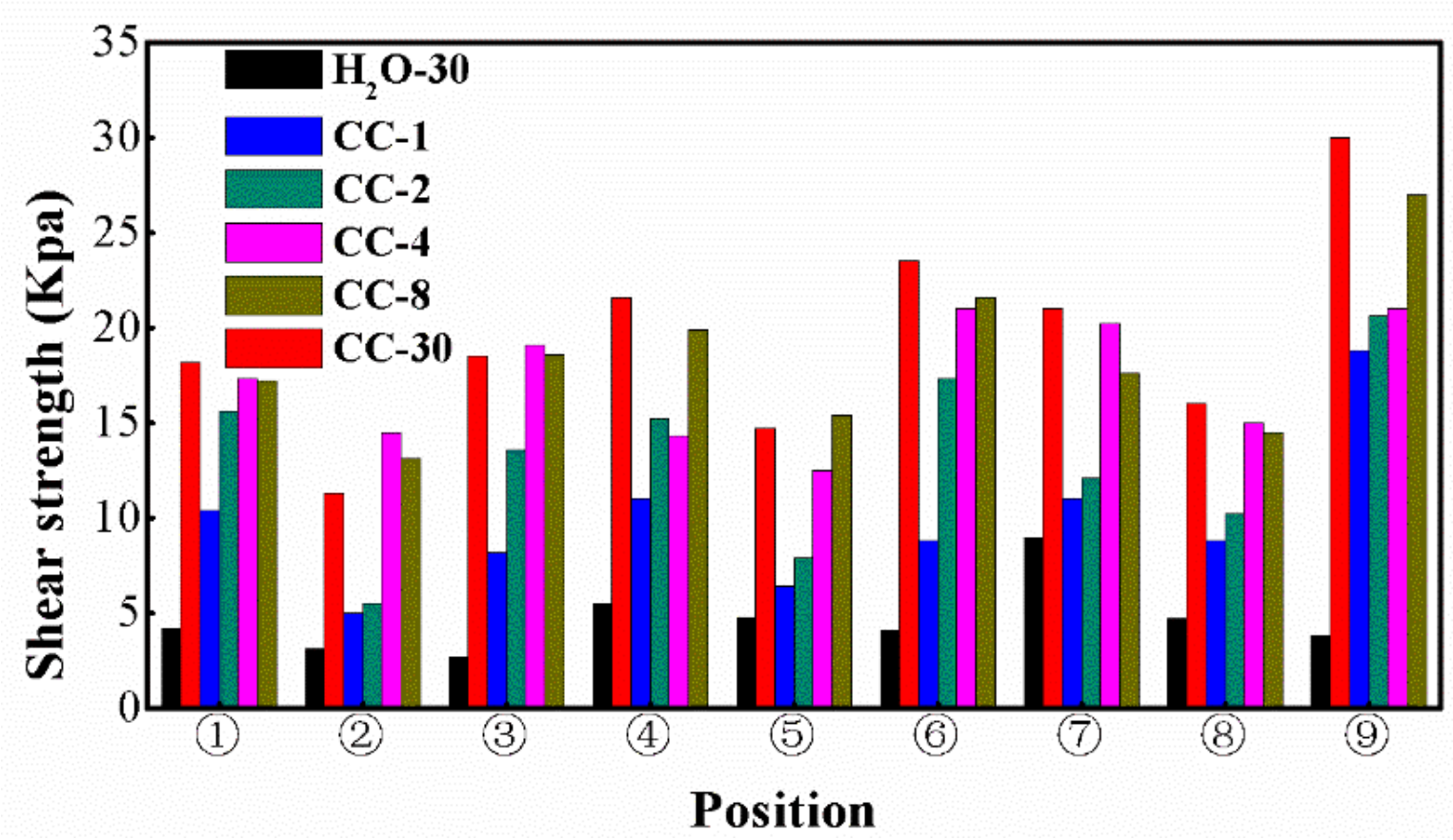

Figure 7. Shear strength of the soils sampled from different positions.

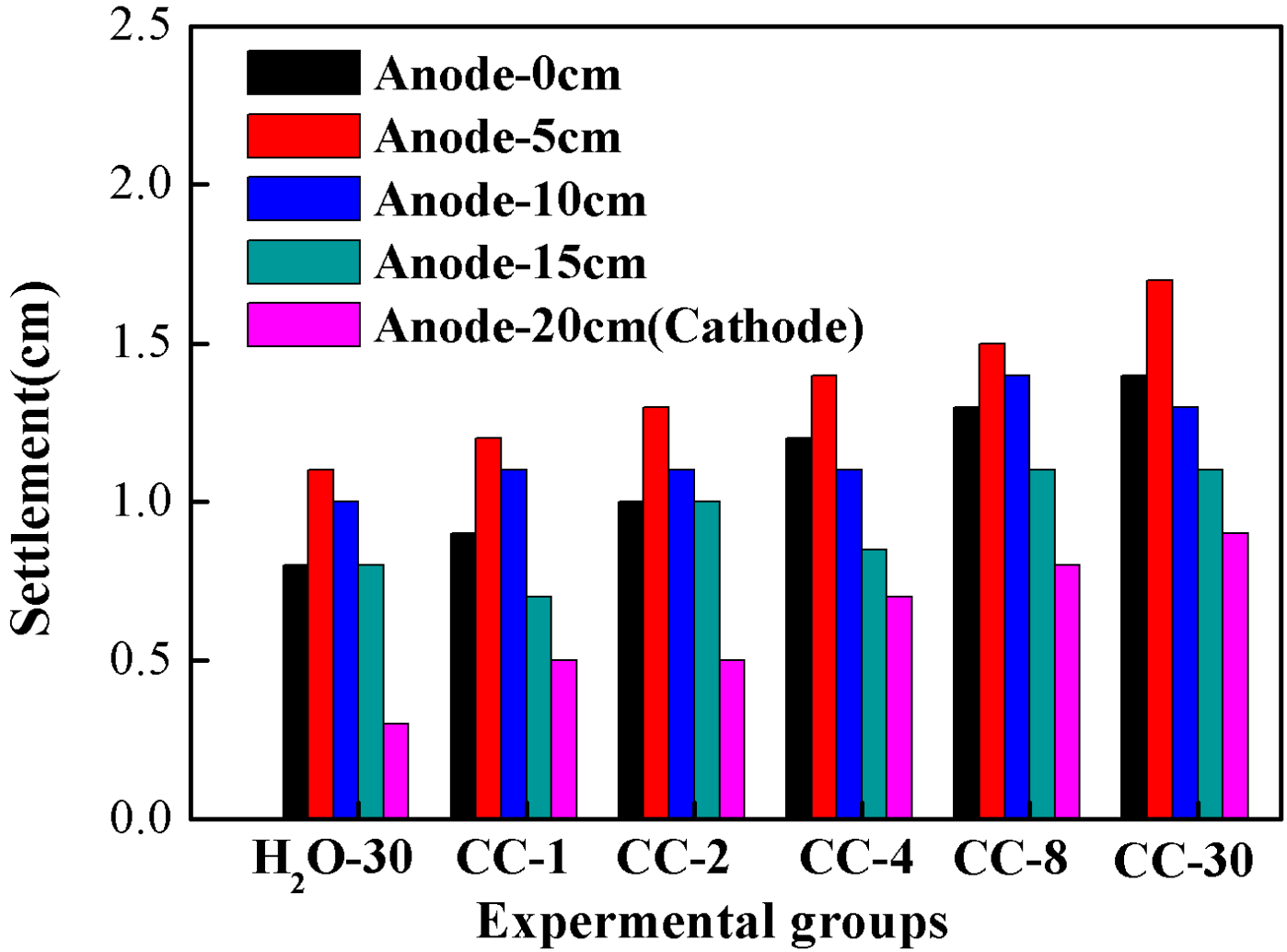

Figure 8. Soil settlement as a function of distance from the anode.

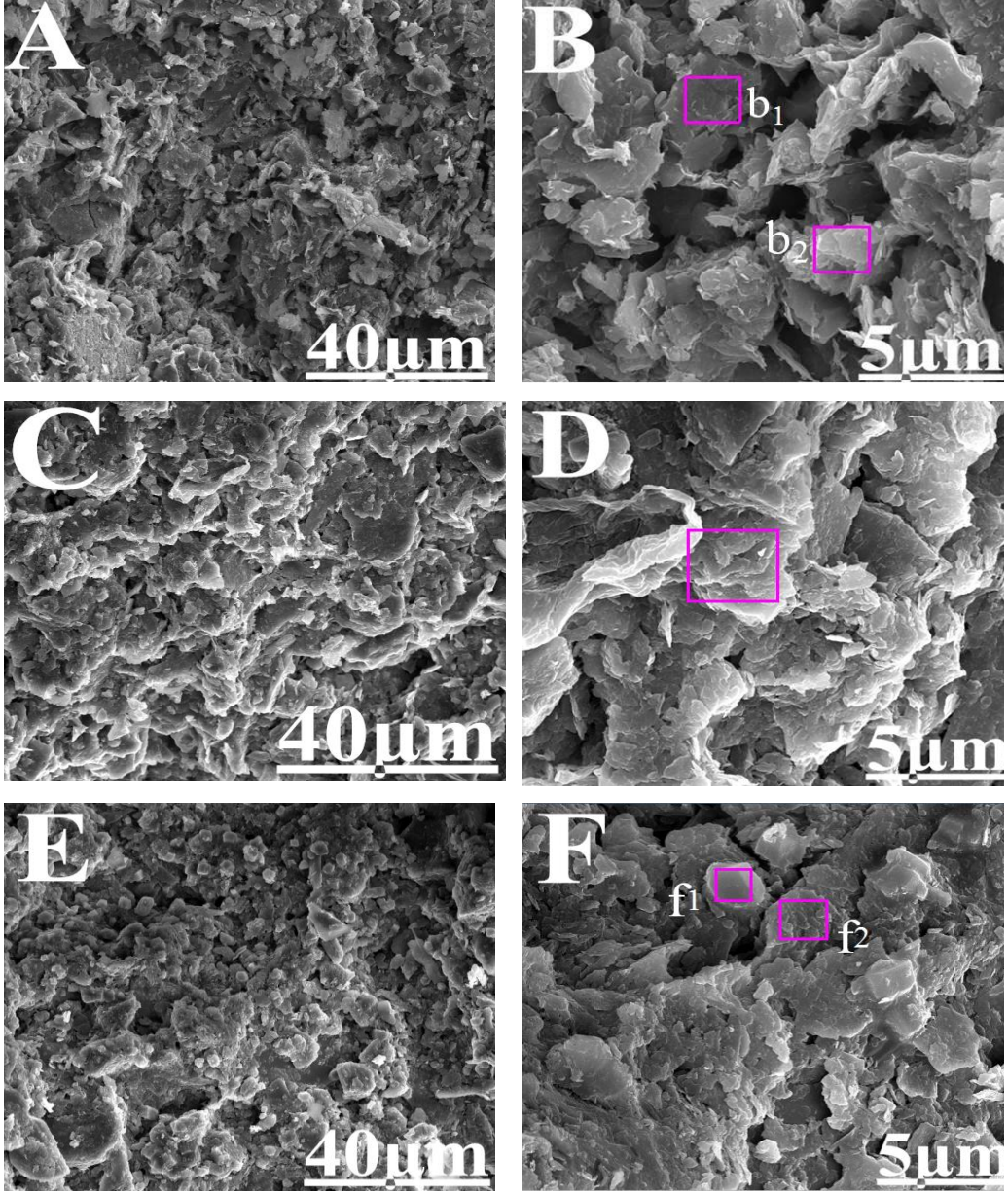

Figure 9. SEM micrographs for various soil samples.

(A, B) Sample H_2O-30; (C, D) Sample CC-30; (E, F) Sample CC-1.

Conclusions

In order to study the complex mechanisms underlying the soil reinforcement by electro-osmosis, we proposed a new electric field condition where the traditional constant potential is partially replaced by alternating pulse wave potentials.

The temporal proportion of the alternating potential was varied to adjust both the pH values of the soil and the dynamic behaviors of the *in situ* formed particles.

By detailed investigation of shear strength, settlement as well as the microstructure of the soil, we reveal that the primary mechanism for the shear strength improvement in the presence of $CaCl_2$ anolyte is not only water drainage but also the *in situ* formation of Ca-rich particles and their inter-connectivity at the microscopic level.

RSC Advances

PAPER

View Article Online
View Journal | View Issue

Cite this: *RSC Adv.*, 2017, 7, 12103

Effect of nanomaterials and electrode configuration on soil consolidation by electroosmosis: experimental and modeling studies

Heng Zhang,[abc] Guoxiang Zhou,[b] Jing Zhong,*[ac] Zhang Shen[b] and Xianming Shi*[bd]

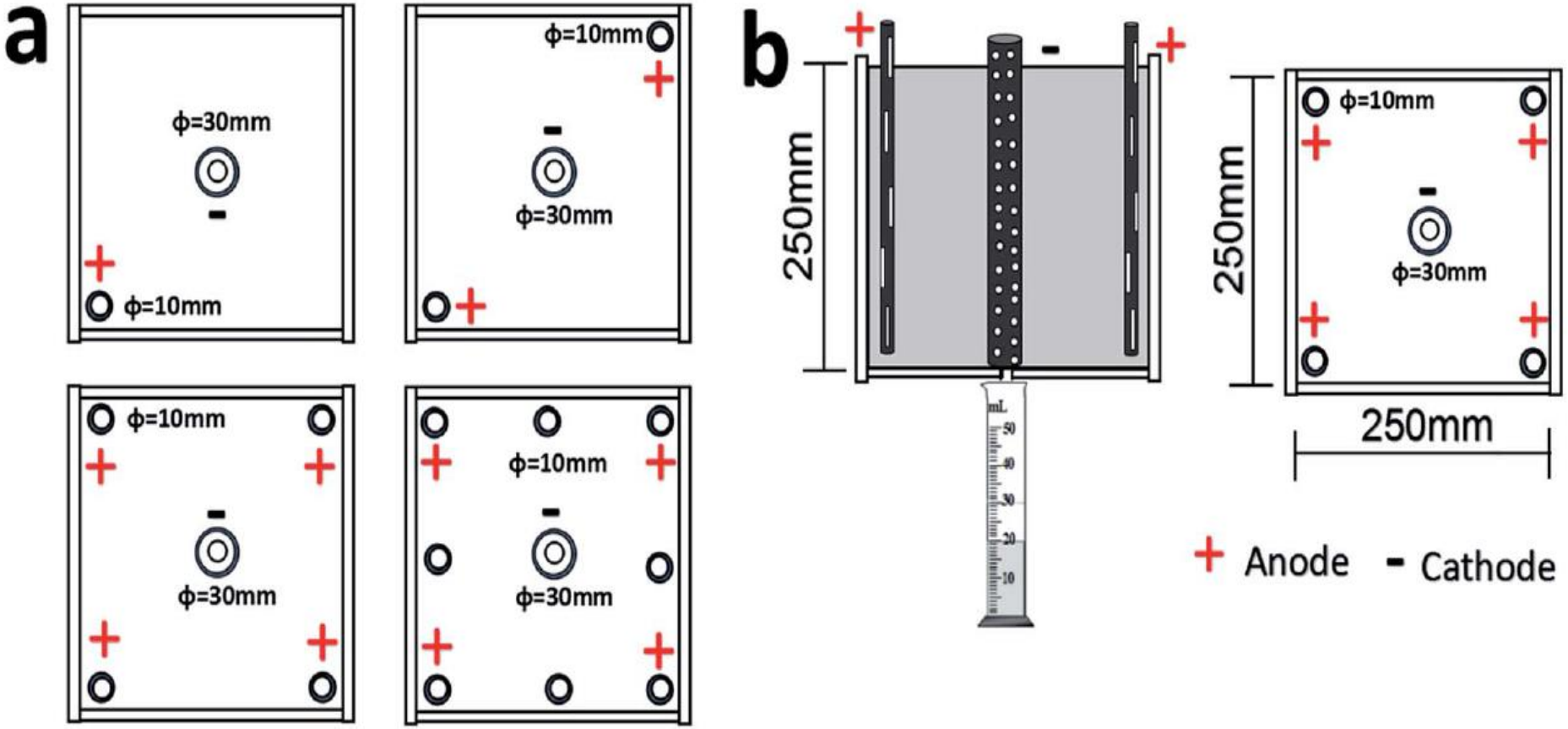

Fig. 1 Schematic configuration of electroosmotic cells (a) top view (b) profile.

Table 1 Physical properties of the as-received soil

Physical properties	
Water content (%)	42.7
Liquid limit (%)	53.7
Plastic limit (%)	21.4
Plastic index	32.3
Specific gravity	2.75

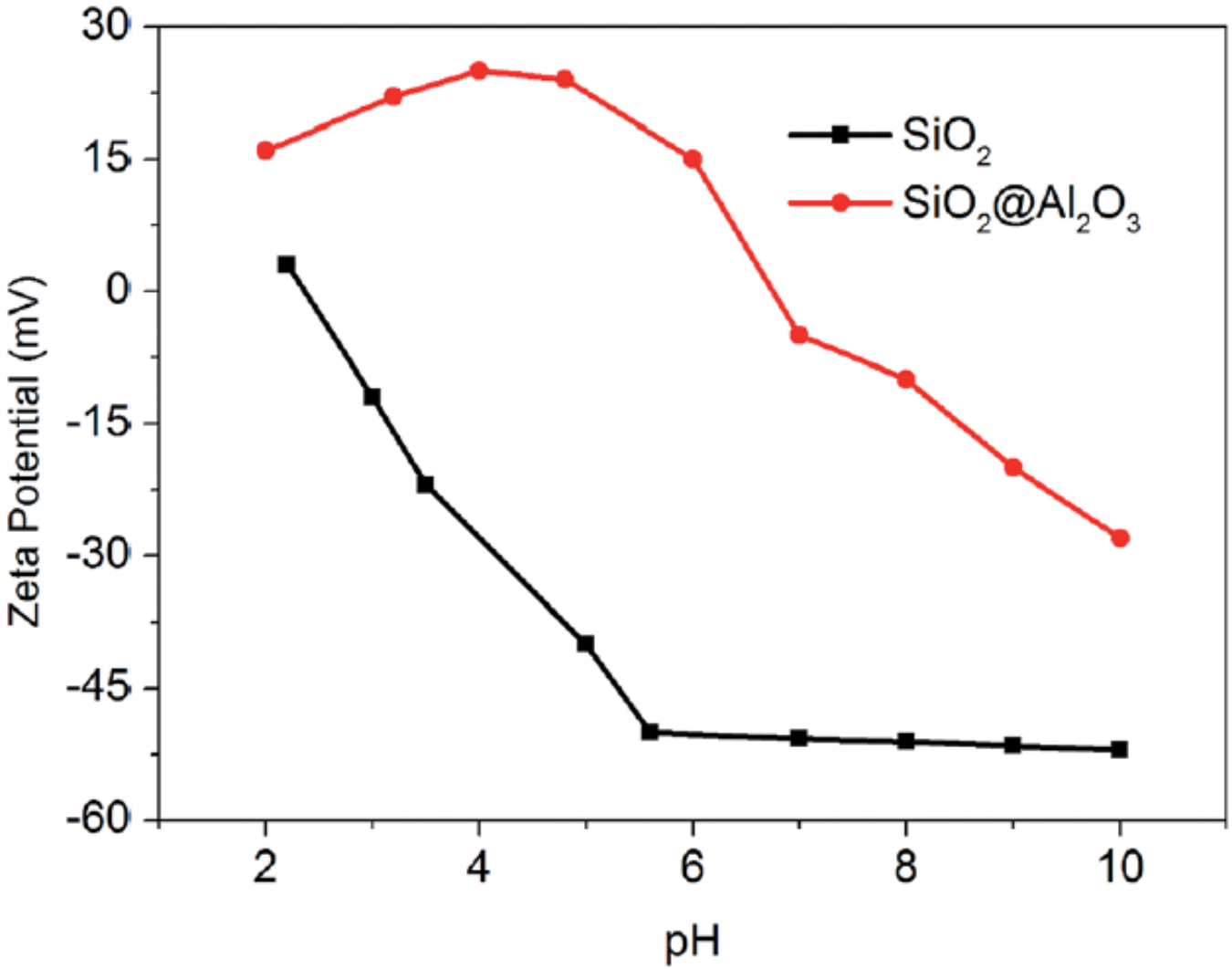

Fig. 2 Zeta potential of SiO_2 NPs *vs.* $SiO_2@Al_2O_3$ core–shell NPs as a function of pH.

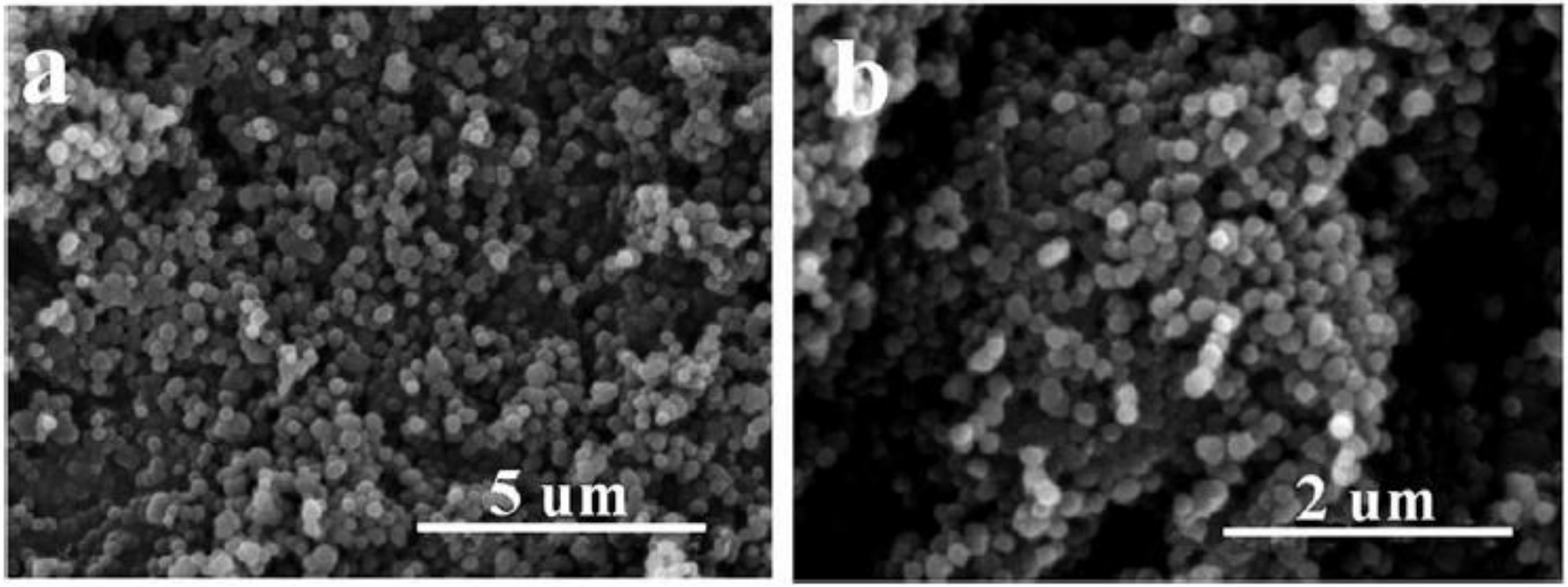

Fig. 3 SEM images of SiO_2 NPs (a) and $SiO_2@Al_2O_3$ core–shell NPs (b).

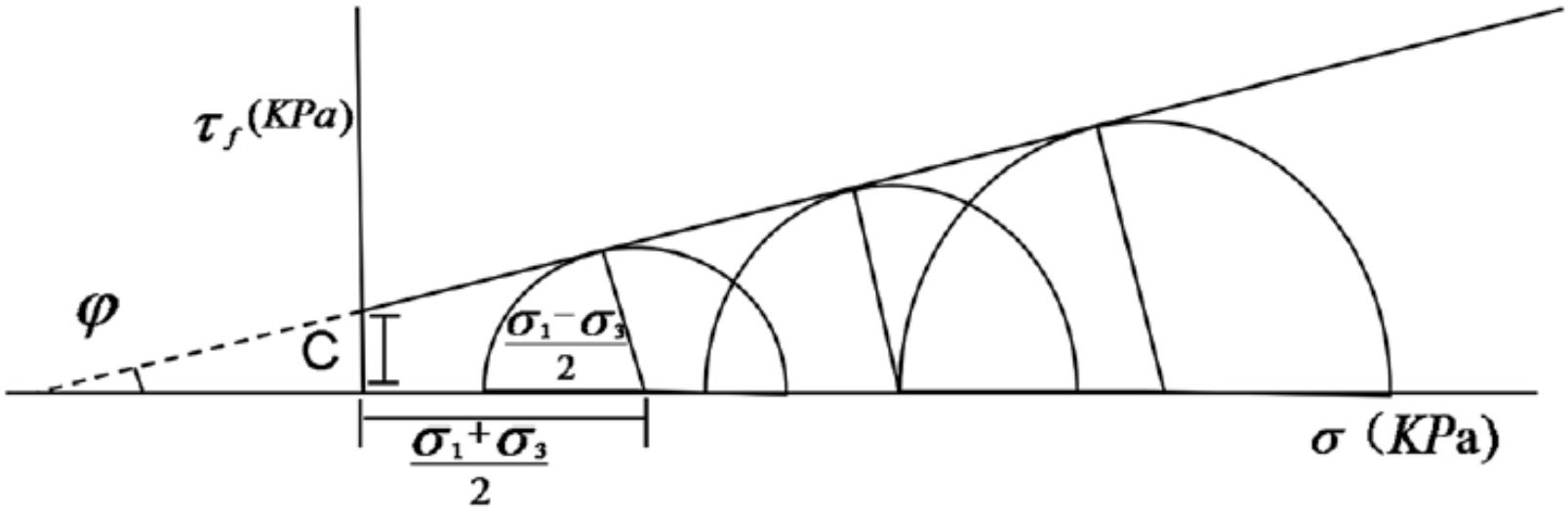

Fig. 4 The schematic for calculating the undrained shear strength (τ_f) of soil, where C denotes the cohesion and φ denotes the friction angle.

Table 2 Parameters used in the numerical investigation

Parameters	Value	Unit
Type of NPs	$SiO_2@Al_2O_3$	—
Applied voltage	20	V
Dielectric constant of NPs[a]	20	—
Dielectric constant of liquid[a]	120	—
Effective porosity of soil[a]	0.5	—
Density of NPs	2.4	$g\ m^{-3}$
Density of soil	1900	$Kg\ m^{-3}$
Density of liquid	1000	$Kg\ m^{-3}$
Initial concentration of NPs	1.0	$Mg\ ml^{-1}$
Diameter of NPs	350	nm
Saturation level of soil	100	%

[a] The value of these parameters was not experimentally measured; instead, a reasonable value was assumed based on domain knowledge. While varying these parameters in a certain range changed the output values of the simulation, it did not change the trends identified in the simulation results.

Table 3 Summary of electroosmotic treatment results. Replicate experiments suggested variabilities within ±7%

Test no.	Solution type	Concentration (mg ml^{-1})	Number of anodes	Shear strength (kPa)				Drained water (ml)	Water content (%)	
				Anode		Cathode				
				C	φ	C	φ		Anode	Cathode
EO1	Water	No	1	4.6	17.3	[a]	[a]	425	45.8	53.9
EO2		No	2	5.2	17.5	[a]	[a]	670	42.4	53.5
EO3		No	4	10	22.8	[a]	[a]	737	41.7	52.3
EO4		No	8	11	23.3	[a]	[a]	887	38.6	50.7
EN1	Core–shell NPs	0.1	1	4.9	17.5	3.1	15.4	521	43.2	53.4
EN2		0.1	2	7	18.2	3.6	16	869	40	52.1
EN3		0.1	4	11	22.6	5.2	18.4	936	37.5	50.7
EN4		0.1	8	12.2	23.6	6.1	19.2	1024	35.2	50
EN5		0.5	1	5.2	18.1	4.1	16.2	617	40.2	53.3
EN6		0.5	2	7.9	19.3	4.8	17.3	991	39.5	51
EN7		0.5	4	11.8	23.8	6.5	19.4	1134	36.3	50.6
EN8		0.5	8	13.2	24.5	7.2	20.3	1231	33.4	48.6
EN9		1.0	1	6.4	19	5.3	17.6	709	38.7	52
EN10		1.0	2	8.5	21.1	6.2	18.6	1143	36	51.3
EN11		1.0	4	12.8	25.3	10.7	22.5	1313	33.8	50
EN12		1.0	8	14.1	26.2	1.4	23.1	1336	31	48

[a] After the electroosmosis of EO samples, the moisture content of soil near the cathode was near 50%, and the soil was almost in a flow condition and its shear strength was too small to measure.

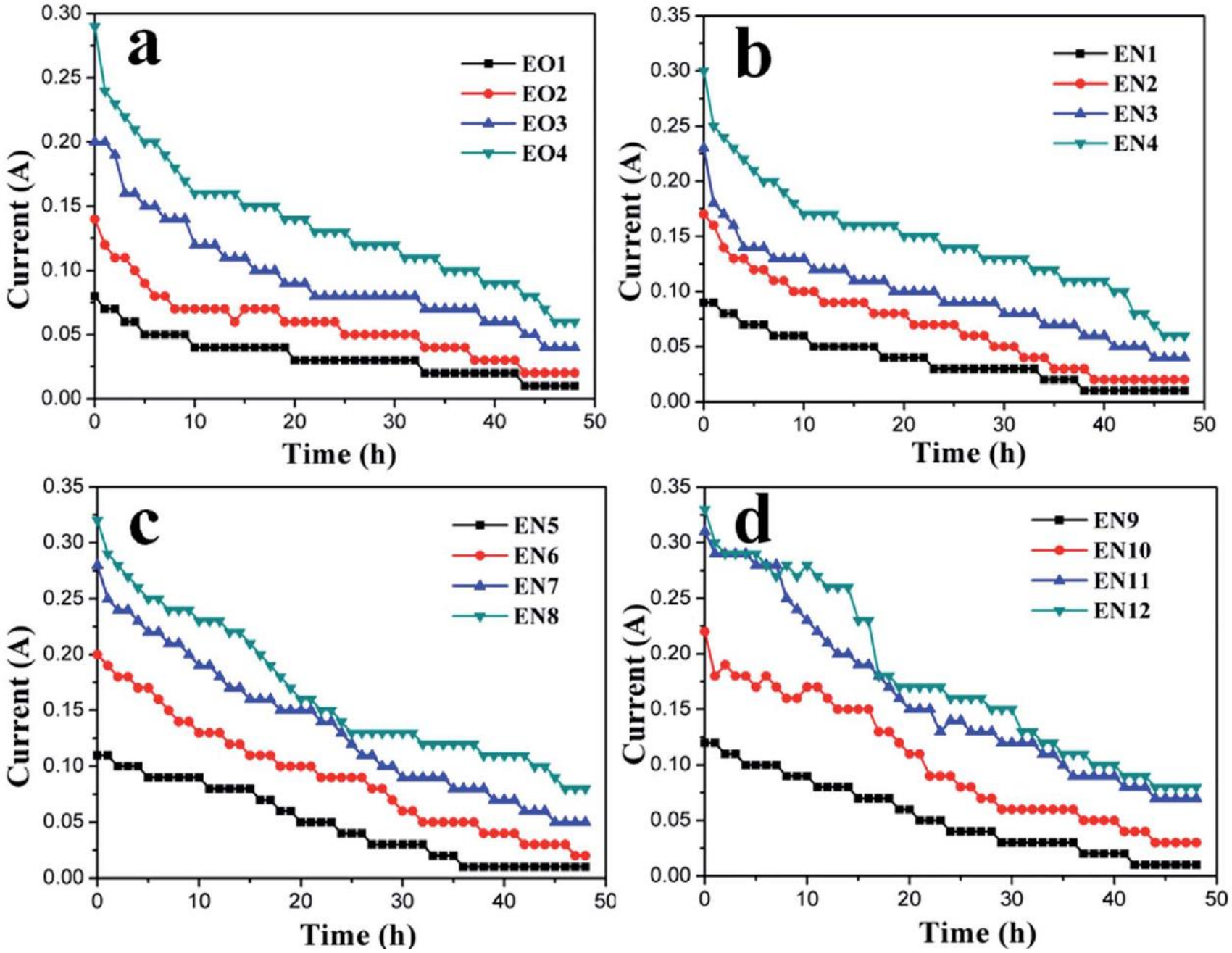

Fig. 5 Evolution of electric current with time during treatment with electroosmosis and injection of positively charged NPs: (a) 0 mg ml^{-1}; (b) 0.1 mg ml^{-1}; (c) 0.5 mg ml^{-1}; (d) 1.0 mg ml^{-1}. Replicate experiments suggested variabilities within ±8%.

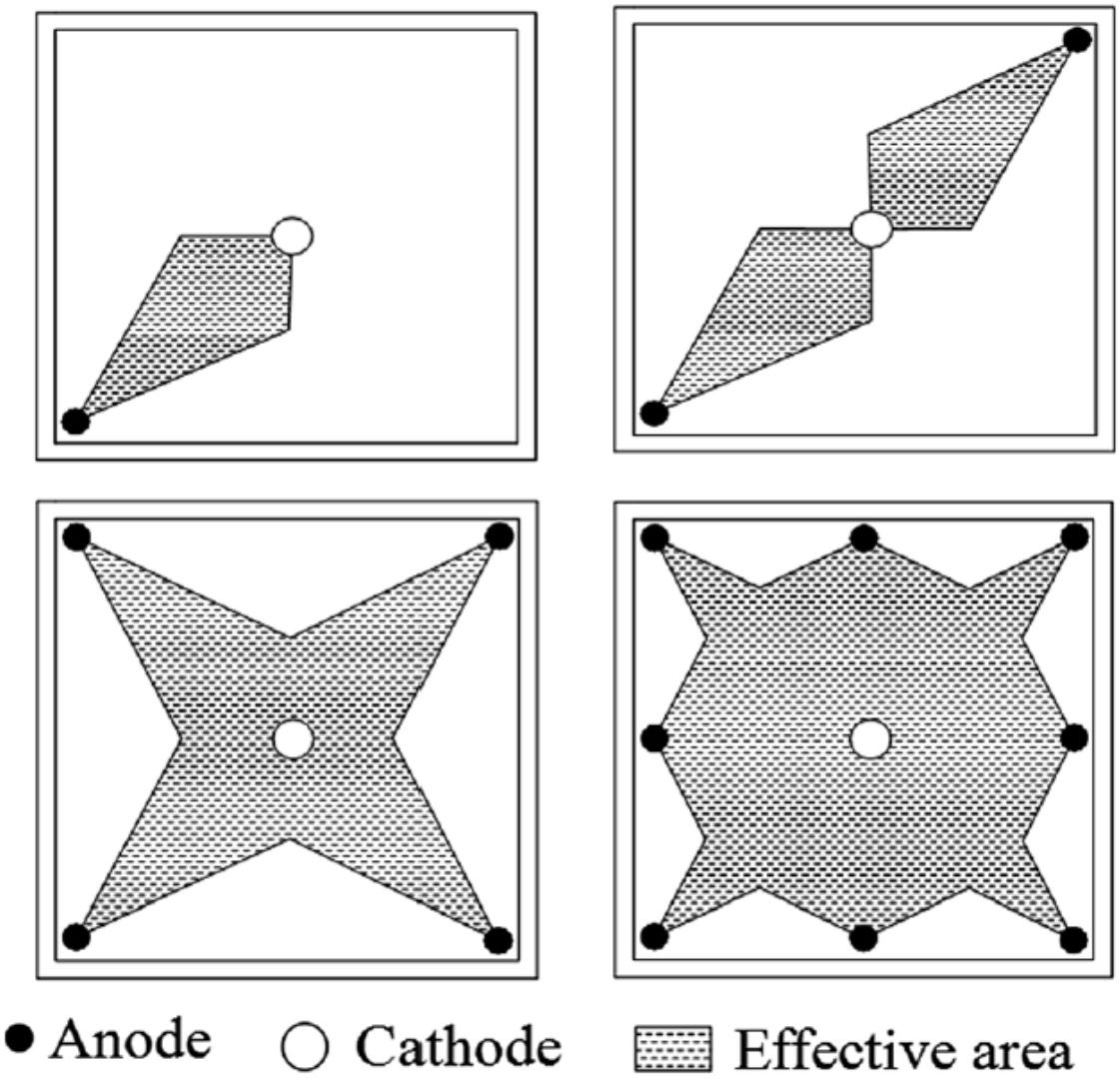

Fig. 6 Schematic illustrating the effect of anode configuration on the distribution of effective area during electroosmosis.[19]

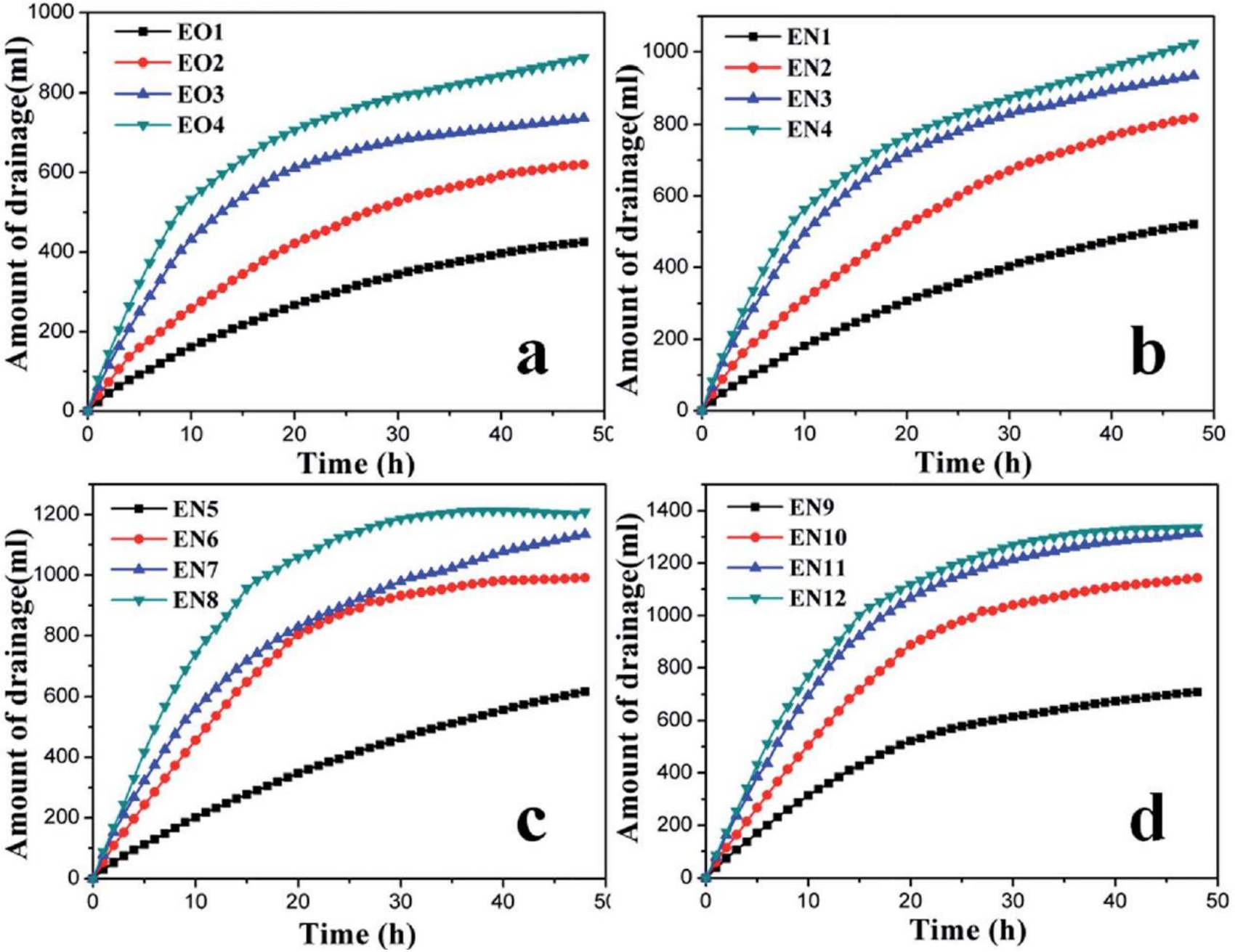

Fig. 7 Evolution of drained water volume with time during treatment with electroosmosis and injection of positively charged NPs: (a) 0 mg ml^{-1}; (b) 0.1 mg ml^{-1}; (c) 0.5 mg ml^{-1}; (d) 1.0 mg ml^{-1}. Replicate experiments suggested variabilities within ±7%.

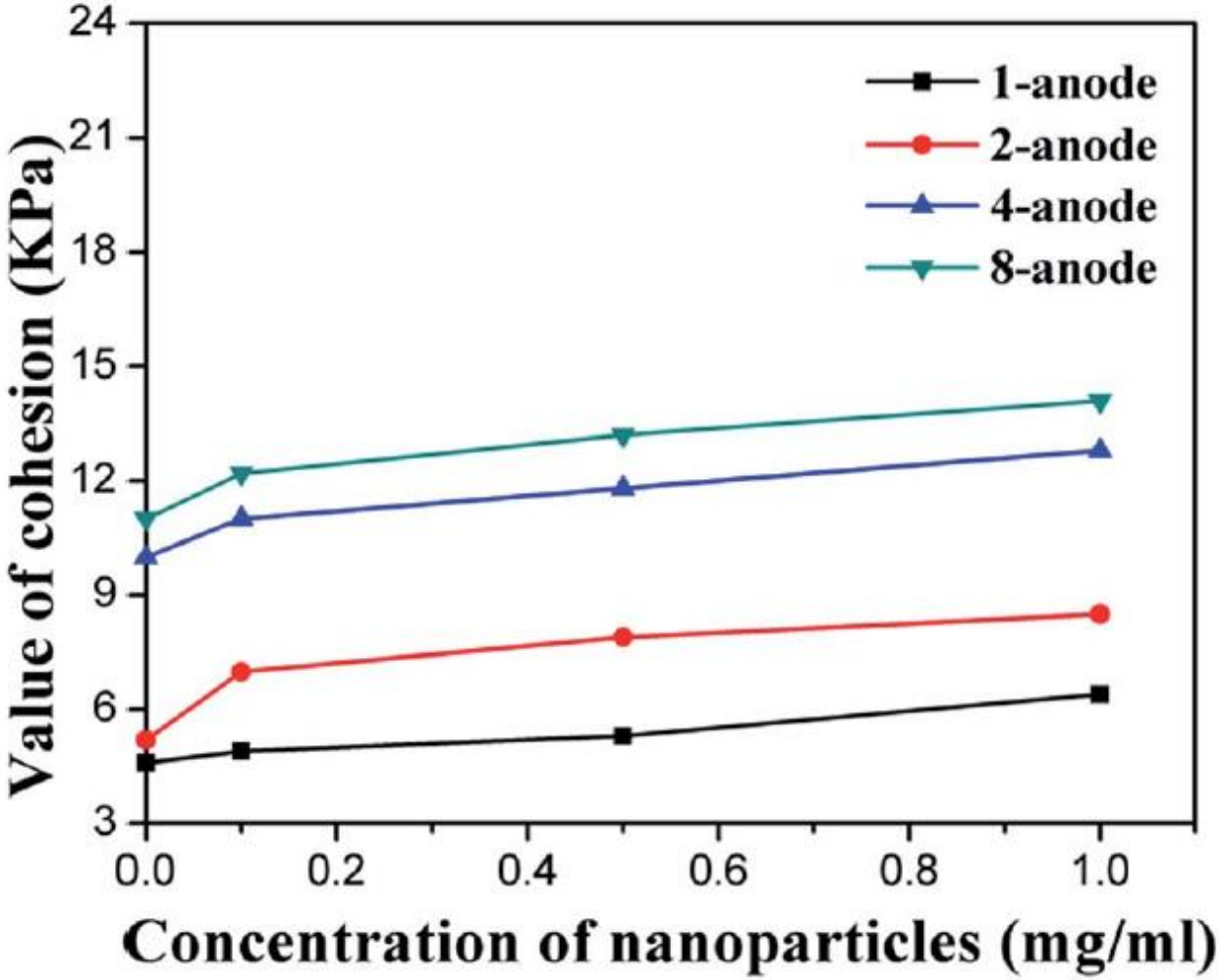

Fig. 8 Increment of the cohesion of soil near the anode due to electroosmosis and NPs injection.

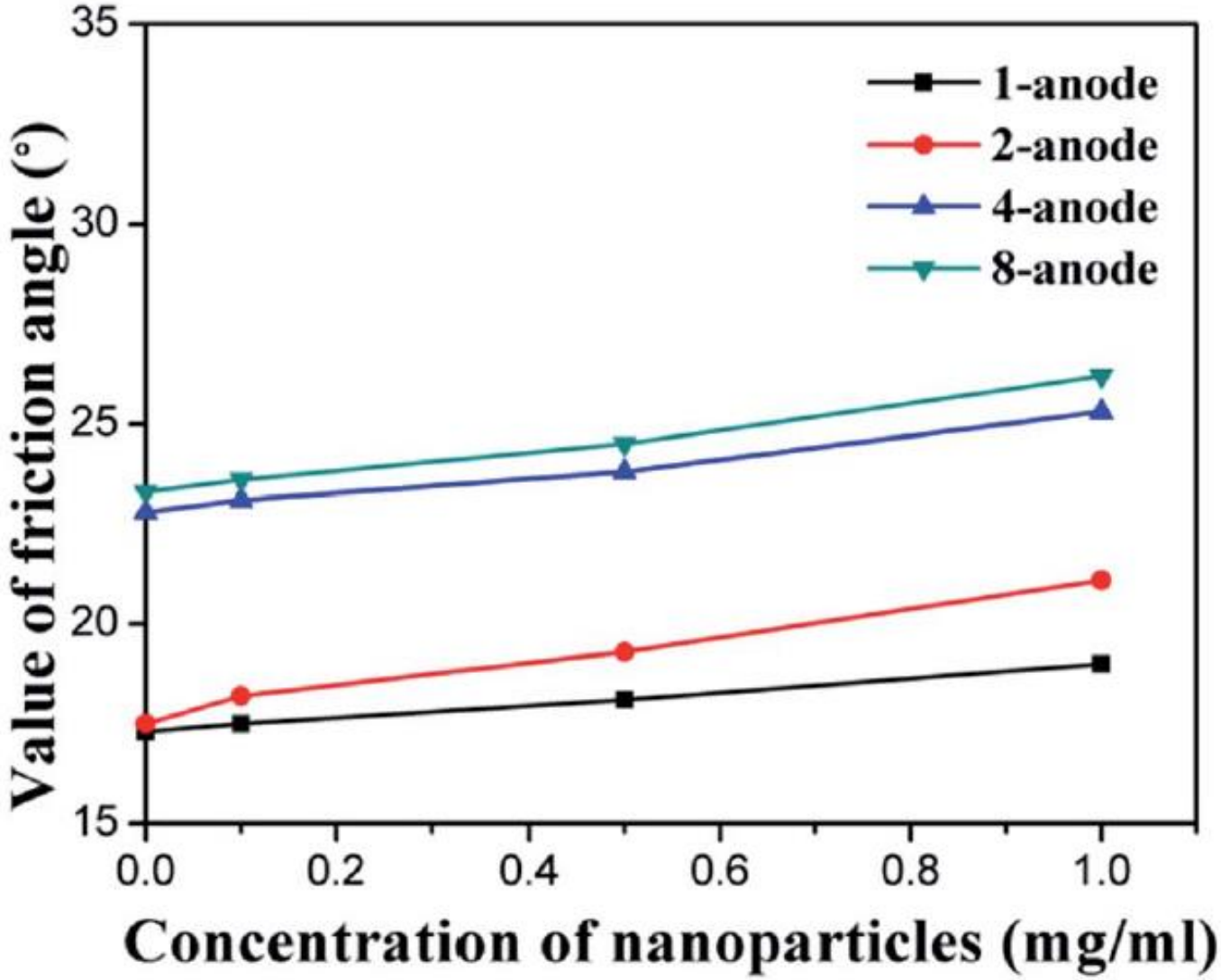

Fig. 9 Increment of the friction angle of soil near the anode due to electroosmosis and NPs injection.

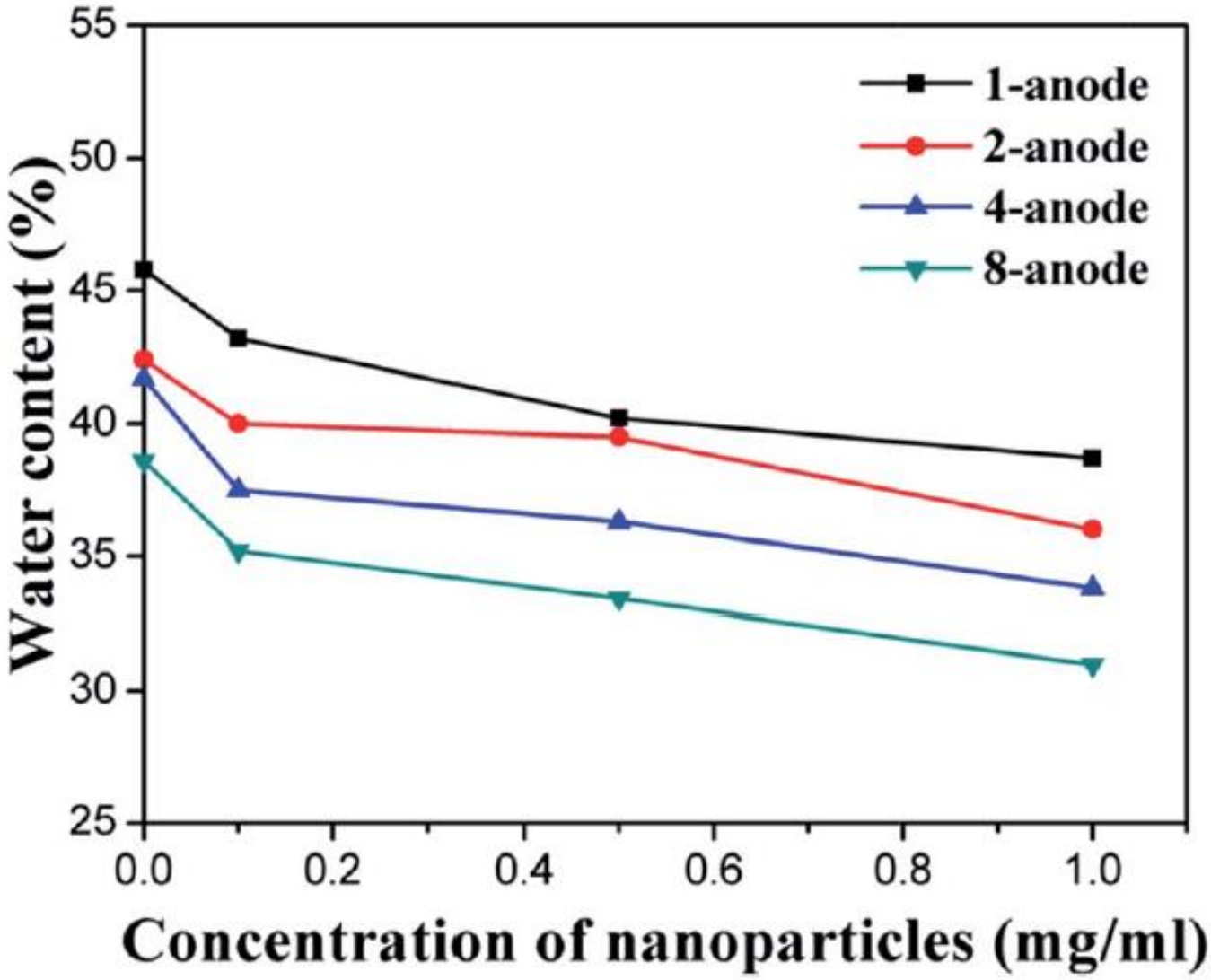

Fig. 10 The water content of the treated soil near the anode, as a function of concentration of NPs.

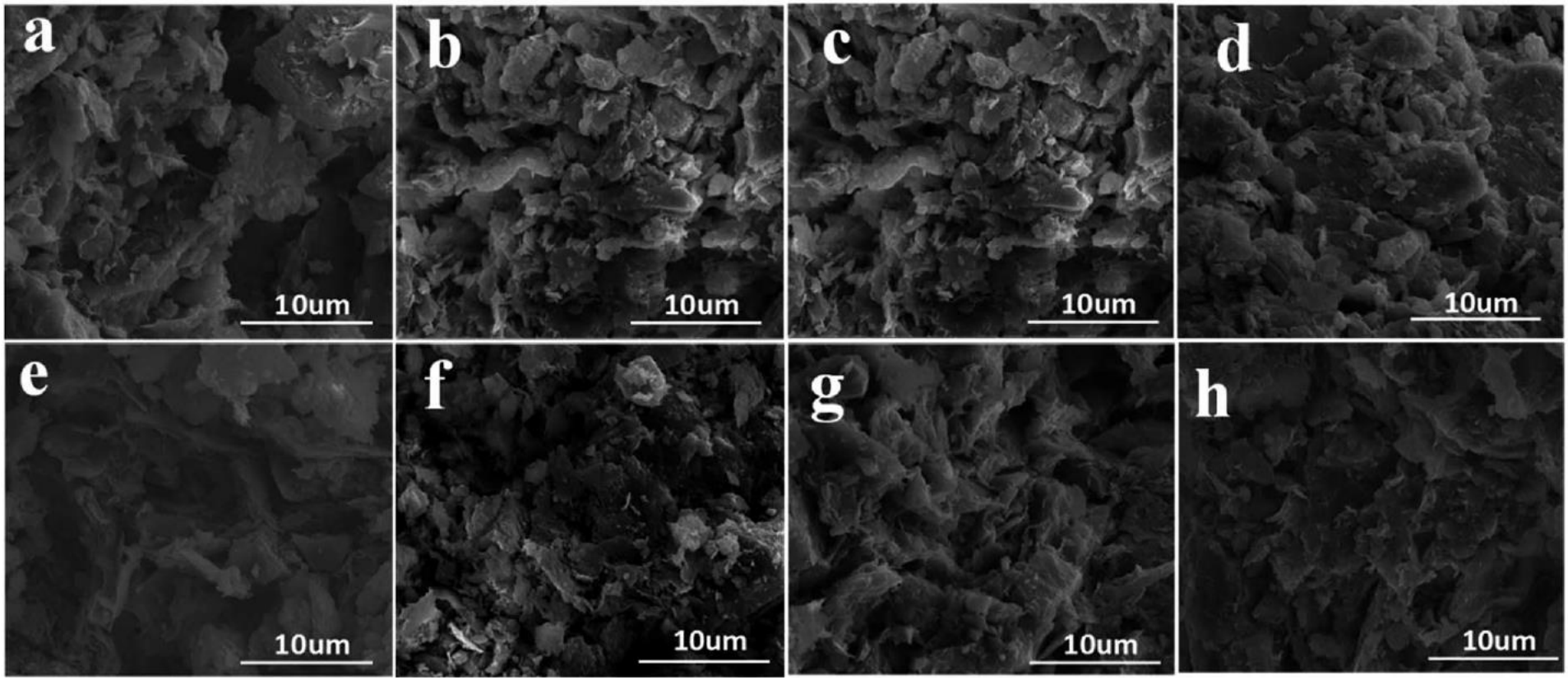

Fig. 11 Representative SEM micrographs of the soil near cathode after electroosmosis only or with injection of positively charged NPs: (a) EO1 (b) EO2 (c) EO3 (d) EO4 (e) EN9 (f) EN10 (g) EN11 (h) EN12.

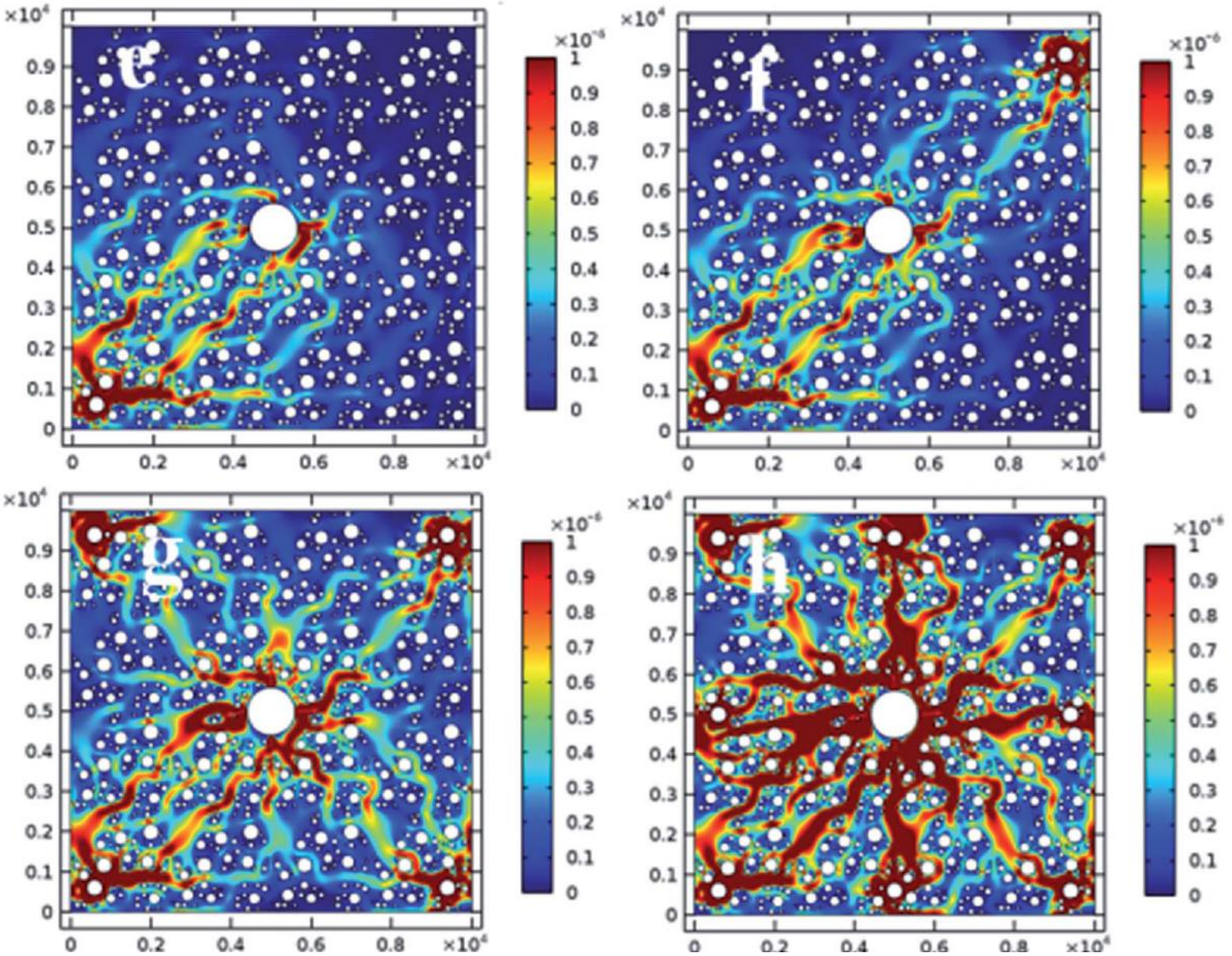

Fig. 12 Variation of electroosmotic coefficient of electroosmosis process with 1 mg ml^{-1} NPs (e–h).

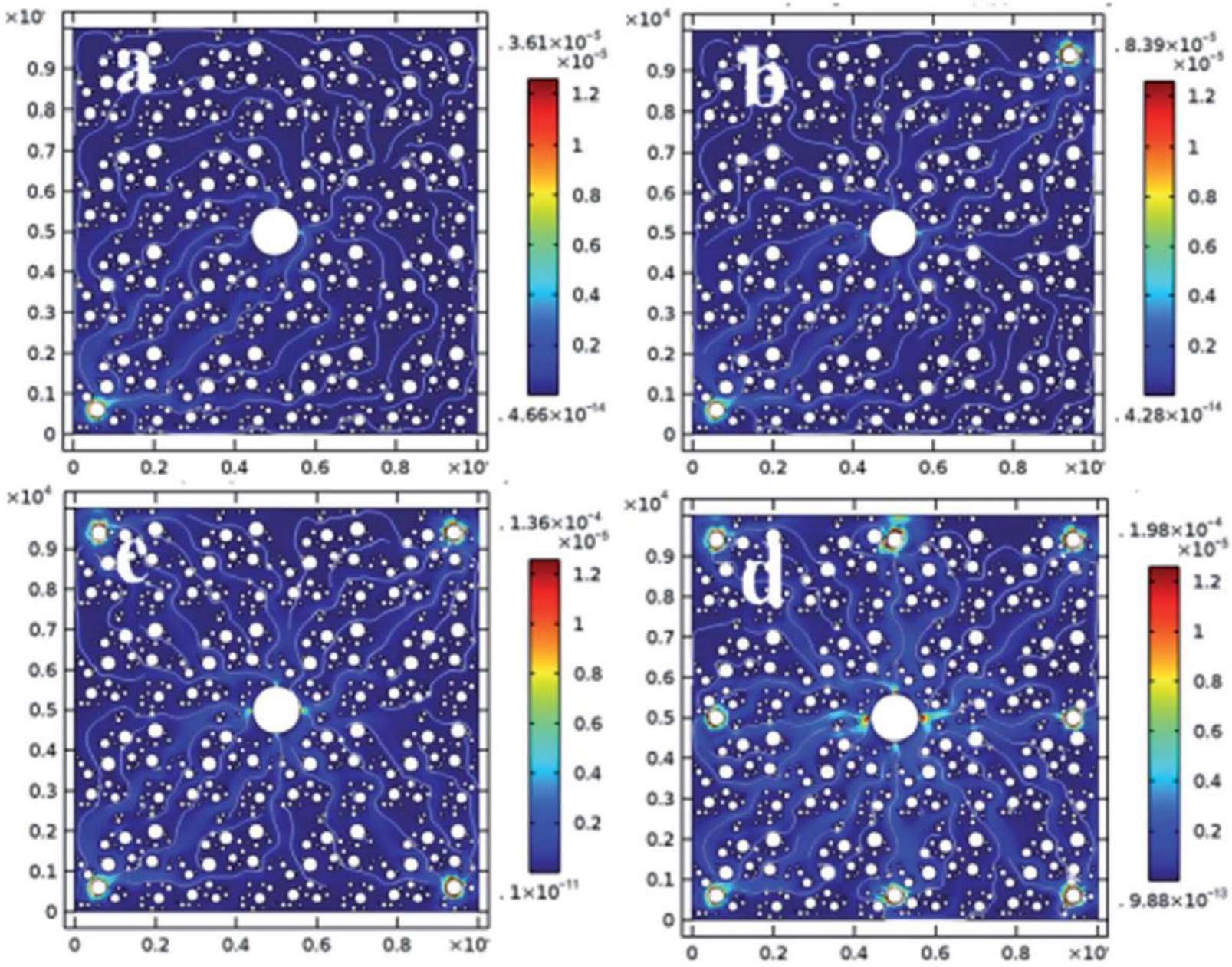

Fig. 12 Variation of electroosmotic coefficient of electroosmosis process without

Conclusions

In this work we adopted different configurations of anodes with the injection of various concentrations of positively charged $SiO_2@Al_2O_3$ core–shell NPs to study the effects of electroosmosis and NPs injection on the dewatering and consolidation of a soil.

(1) Regardless of the absence or presence of NPs, both the electric current and the time efficiency of soil dewatering increased with the number of anodes per cathode, which can be attributed to the more uniform and larger effective electric field formed in the soil (lake silt). This translated to denser microstructure and improved cohesion and friction angle of the soil.

(2) The addition of NPs further enhanced the electric current and drainage efficiency during electroosmosis, which increased with the concentration of the NP suspension.

Future Direction of This Work

- Treatment of anode to minimize its corrosion and interfacial resistance
- Vacuumed compression pretreatment + nano-electroosmosis
- Geo-environmental engineering: removal of soil pollutants
- …

Questions?

Xianming Shi, PhD, PE

Civil & Environmental Engineering

Washington State University

Sloan 101, PO Box 642910

Pullman, WA 99164-2910

Phone: 1-509-335-7088

xianming.shi@wsu.edu

http://public.wsu.edu/~xianming.shi/

Center for Environmentally Sustainable Transportation in Cold Climates

CESTiCC

WASHINGTON STATE UNIVERSITY

武漢輕工大學

WUHAN POLYTECHNIC UNIVERSITY

1951